



1 **Geosphere Coupling and Hydrothermal Anomalies before the 2009 Mw 6.3**

2 **L'Aquila Earthquake in Italy**

3 L.X. Wu^{1,5*}, S. Zheng², A. De Santis³, K. Qin¹, R. Di Mauro⁴, S.J. Liu⁵ and M. L.
4 Rainone⁴

5 *1 School of Environment Science and Spatial Informatics, China University of Mining*
6 *and Technology, Xuzhou, China*

7 *2 Academy of Disaster Reduction & Emergency Management, Beijing Normal*
8 *University, Beijing, China*

9 *3 Istituto Nazionale di Geofisica e Vulcanologia, Sezione Roma 2, Roma, Italy*

10 *4 Dipartimento di Ingegneria e Geologia, Chieti University, V. Vestini 31, 66013*
11 *Chieti Scalo, Italy*

12 *5 Northeast University, Shenyang, China*

13 *Corresponding author: Lixin Wu,

14 School of Environment Science and Spatial Informatics, China University of Mining
15 and Technology, Xuzhou, China;

16 Email: awulixin@263.net, wlx@cumt.edu.cn

17 **Abstract:** The earthquake (EQ) anomalies associated with the April 6, 2009 Mw 6.3
18 L'Aquila EQ have been widely reported. Nevertheless, the reported anomalies have
19 not been so far synergically analyzed to interpret or prove the potential LCA coupling
20 process. Previous studies on *b*-value are also insufficient. In this work, the
21 spatio-temporal evolution of several hydrothermal parameters related to the
22 coversphere and atmosphere, including soil moisture, soil temperature, near-surface
23 air temperature, and precipitable water, was comprehensively investigated. Air
24 temperature and atmospheric aerosol were also statistically analyzed in time series
25 with ground observations. An abnormal enhancement of aerosol occurred on March
26 30, 2009 and thus proved quasi-synchronous anomalies among the hydrothermal
27 parameters from March 29 to 31 in particular places geo-related to tectonic thrusts and
28 local topography. The three-dimensional (3D) visualization analysis of *b*-value
29 revealed that regional stress accumulated to a high level, particularly in the L'Aquila
30 basin and around regional large thrusts. Finally, the coupling effects of geospheres
31 were discussed, and a conceptual LCA coupling mode was proposed to interpret the
32 possible mechanisms of the multiple quasi-synchronous anomalies preceding the
33 L'Aquila EQ. Results indicate that CO₂-rich fluids in deep crust might have played a
34 significant role in the local LCA coupling process.



35 **1. Introduction**

36 The thermal anomalies occurring before large and hazardous earthquakes (EQs) have
37 been extensively observed from satellites or on the Earth's surface. In particular,
38 several thermal parameters, including thermal infrared radiation (TIR) [Tronin et al.,
39 2002; Saraf and Choudhury, 2004], surface latent heat flux [Dey and Singh, 2003; Qin
40 et al., 2012, 2014a], and outgoing longwave radiation [Ouzounov et al., 2007; Jing et
41 al., 2012], have been proven to be related to tectonic seismic activities. With the
42 development of Earth observation technologies and anomaly recognition methods
43 [e.g., Wu et al., 2012; Qin et al., 2013], non-thermal anomalous variations in
44 geochemical and electromagnetic signals from different spheres of the Earth may
45 indicate complex geosphere coupling effects during the slow preparation phase of
46 EQs. During the past decades, several mechanisms or hypotheses for interpreting
47 thermal anomalies have been proposed; examples include the positive hole (P-hole)
48 effect [Freund, 2011], transient electric field [Liperovsky et al., 2008], frictional heat
49 of faults [Geng et al., 1998; Wu et al., 2006], and the greenhouse effect caused by
50 Earth degassing [Tronin et al., 2002]. A unified lithosphere–atmosphere–ionosphere
51 coupling model was proposed to explain the inherent links among different
52 parameters [Liperovsky et al., 2008a; Pulinets and Ouzounov, 2011; Pulinets, 2012].
53 This model has been verified by several case studies on the spatio-temporal features
54 of the anomalies of multiple parameters [Pulinets et al., 2006; Zheng et al., 2014]. Wu
55 et al. [2012] emphasized not only the effect of the coversphere (including water
56 bodies, soil/sand layers, deserts, and vegetation on the Earth's surface) on pre-EQ
57 anomalies but also the importance of this transition layer from the lithosphere to the
58 atmosphere. The coversphere performs the vital functions of producing observable
59 signals and enlarging or reducing the transmission of electric, magnetic,
60 electromagnetic, and thermal signals from the lithosphere to the atmosphere, and even
61 to satellite sensors. Although the existence of many diagnostic precursors, such as
62 crustal strain, seismic velocity, hydrological change, gas emission and
63 electromagnetic signals, and their usefulness for earthquake forecasting is still



64 controversial [Cicerone et al 2009; Jordan et al 2011]. With the abundant data such
65 provided by Global Earth Observation System of System (GEOSS), multiple
66 parameters from the integrated Earth observation should be encouraged to test for
67 earthquake anomaly recognition and advance knowledge of precursor signals. The
68 2009 Mw6.3 L'Aquila EQ may provide an ideal opportunity for us to further cognize
69 various change of observational signals in geosphere system and understand their
70 possible link with geophysical survey.

71 A Mw 6.3 EQ struck the Abruzzi region in central Italy on April 6, 2009 (01:32 UTC),
72 and its epicenter was located at 42.34 °N/13.38 °E (depth of 9.5 km), which was near
73 the city of L'Aquila (Fig.1). According to the Istituto Nazionale di Geofisica e
74 Vulcanologia (INGV), many strong foreshocks had been occurring since December
75 2008, and more than 10,000 aftershocks had been recorded until September 2010.
76 Previous geological studies stated that the present-day geologic setting along the
77 Italian peninsula related to the N-S convergence zone between the African and the
78 Eurasian plates is particularly complex because different processes occur
79 simultaneously and in close proximity [Montone et al., 2004; Galadini et al., 2000].
80 Central Italy experiences active NE-SW extensional tectonics approximately
81 perpendicular to the Apenninic fold and thrust belt [Montone et al., 2012]; a city in
82 this region is L'Aquila, which is bounded by the *Olevano–Antrodoco* and *Gran Sasso*
83 thrusts at the west and north sides, respectively. In 2009, the L'Aquila main shock
84 occurred as a result of normal faulting (*Paganica* fault, PF) and as a primary response
85 to the Tyrrhenian basin opening faster than the compression between the Eurasian and
86 African plates [USGS, 2009].

87 A large number of the precursory anomalies of the 2009 L'Aquila EQ were reported
88 after the main shock. These anomalous parameters included thermal properties,
89 electric and magnetic fields, gas emissions, and seismicity [Akhoondzadeh et al., 2010;
90 Biagi et al., 2009; Bonfanti et al., 2012; Cianchini et al., 2012; De Santis et al., 2011;
91 Eftaxias et al., 2009; Genzano et al., 2009; Gregori et al., 2010; Lisi et al., 2010;
92 Papadopoulos et al., 2010; Piroddi and Ranieri, 2012; Plastino et al., 2010; Pulineti et
93 al., 2010; Rozhnoi et al., 2009; Tsolis and Xenos, 2010]. Many of the existing reports



94 revealed the existence of temporal quasi-synchronism among the several anomalies of
95 different parameters related to different geospheres (Table 1). We believe that the
96 geosphere coupling effects could support or interpret the occurrence of the various
97 precursory anomalies of the 2009 L'Aquila EQ. Moreover, we hypothesize the
98 possible role of the coversphere in the process of lithosphere–coversphere–
99 atmosphere (LCA) coupling, in which the radiation transmission caused anomalous
100 thermal infrared signals in satellite sensors.

101 Air ionization and ion hydration are generally known as critical physical processes
102 that result in different types of EQ precursors between the ground surface and the
103 lower atmosphere [Pulinets and Ouzounov, 2011; Freund, 2011]. However, a
104 corresponding observation of complementary parameters related to the coversphere,
105 such as humidity, water vapor, heat flux, and atmospheric aerosol, is not
106 comprehensive enough to obtain a plain validation.

107 The seismic b -value describes the fundamental relationship between the frequency
108 and the magnitude of EQs, which is known as the Gutenberg–Richter law [Gutenberg
109 and Richter, 1944], and is widely applied in tectonic seismicity studies. The b -value
110 represents the size distribution of abundant seismic events of small to moderate
111 magnitudes; it is associated with several physical properties, such as regional stress,
112 material homogeneity, and temperature gradient [Gulia and Wiemer, 2010; Mogi,
113 1962; Schorlemmer et al., 2005; Schorlemmer and Wiemer, 2004, 2005; Tormann et
114 al., 2015; Urbancic et al., 1992; Warren and Latham, 1970; Wiemer and Wyss, 2002;
115 Wyss and Wiemer, 2000]. Hence, the b -value is possibly a proxy of crust stress
116 conditions and could therefore act as a crude stress meter for seismicity observed in
117 the lithosphere [Tormann et al., 2014]. Although the time sequence of the b -value
118 based on microseismicity data before and after the 2009 L'Aquila EQ has been
119 analyzed and has revealed the quasi-synchronous features of the b -value relative to
120 other parameters [De Santis et al., 2011], the correlations of various anomalies in the
121 coversphere and lithosphere remain unclear because of the absence of essential
122 geospatial analysis. Moreover, various factors directly influence the thermal radiation
123 signals observed by satellite sensors; these factors include atmosphere properties



124 (absorption, scattering, and emission of water vapor, as well as aerosol particles),
125 thermal condition of the Earth's surface (meteorological condition, soil moisture and
126 components, vegetation cover, and surface roughness), and the complex thermal
127 process of geo-objects. In view of remote sensing physics and the LCA coupling
128 effect, we have reason to believe that other parameters characterized by the
129 above-mentioned factors in relation to the coversphere and atmosphere should have
130 presented temporal quasi-synchronism and spatial consistency with the reported
131 thermal anomalies before the main shock of the 2009 L'Aquila EQ.

132 Several hydrothermal parameters related to the coversphere and atmosphere,
133 including soil water and temperature, precipitable water, air temperature, and
134 atmospheric aerosol, are comprehensively analyzed in this study to explore the
135 possible coupling effects preceding the 2009 Mw 6.3 L'Aquila EQ. The 3D dynamic
136 evolution of the *b*-value is also analyzed to further investigate the potential
137 correlations of multiple parameter anomalies related to the coversphere and the
138 dynamics of the lithosphere. Furthermore, the variation of some parameters after the
139 main shock is analyzed for comparison. From retrospective analyses of data collected
140 prior to this earthquake, we finally attempt to discuss the geosphere coupling process
141 and propose a model for interpreting the coupling effects with the support of previous
142 geophysical researches.

143 **2. Analysis of hydrothermal parameters**

144 **2.1 Data and method**

145 Four parameters related to the coversphere and atmosphere, namely, volumetric soil
146 moisture level 1 (SML1) at 0–7 cm below ground level, soil temperature level 1
147 (STL1) at 0–7 cm below ground level, near-surface air temperature at a height of 2 m
148 (TMP2m), and precipitable water of the entire atmosphere column (PWATclm), were
149 analyzed in long-term intervals and within two months before and after the main
150 shock. The six-hourly values of the SML1 and STL1 parameters were 00:00, 06:00,
151 12:00, and 18:00 every day according to ERA-Interim, which is a series of the latest
152 global atmospheric reanalysis products produced by the European Centre for



153 Medium-Range Weather Forecasts to replace the ERA-40. The gridded data were
154 transformed into a regular 512° longitude by 256° latitude N128 Gaussian grid with
155 $0.71^\circ \times 0.71^\circ$ spatial resolution (<http://apps.ecmwf.int/datasets/data>). The TMP2m and
156 PWATclm datasets also comprised six-hourly values based on the Final (FNL)
157 Operational Global Analysis system of the National Center for Environmental
158 Prediction (NCEP), which was produced with the same NCEP model as that used for
159 the Global Forecast System (<http://rda.ucar.edu/datasets>). The NCEP-FNL data were
160 also represented in a Gaussian grid with $1^\circ \times 1^\circ$ spatial resolution (360° longitude by
161 181° latitude). All the data from March and April 2000-2009 were investigated. The
162 datasets containing information on the air temperature and aerosol optical depth
163 (AOD) from ground-based observations were considered and compared with the
164 results from the assimilation data to verify the key coupling process of the anomalies.
165 The air temperature data were obtained from the L'Aquila weather station
166 ($42.22^\circ \text{N}/13.21^\circ \text{E}$, elevation of 680 m, shown as yellow circle in Fig. 1), whereas the
167 AOD data were obtained from the Roma station ($41.84^\circ \text{N}/12.65^\circ \text{E}$, elevation of 130 m,
168 shown as yellow triangle in Fig. 1) of the Aerosol Robotic Networks (AERONET,
169 <http://aeronet.gsfc.nasa.gov/>). With respect to the epicenter, the Roma station, which
170 uses the Cimel Electronique CE318 sunphotometer to measure aerosol optical
171 properties, is the only nearby station with available data.

172 First, we analyzed the long time series of the SML1, STL1, TMP2m, and PWATclm
173 data on the epicenter pixel (42.34°N , 13.38°E , shown as black rectangular boxes in
174 Figs. 2.2-2.5). To compare the data in 2009 with historical data, the mean (μ) and
175 standard deviation (σ) were calculated using data from multiple years (2000–2008).
176 Here, an deviation with overquantity more than $\mu+1.5\sigma$ threshold was defined as an
177 alternative anomaly for each parameter on the epicenter pixel. For confutation
178 analysis, we also compared the 2009 data with the data from 2006 (green line in Fig.
179 2), which is regarded as a silent year for its seismicity rate (≤ 10 EQs with M3+
180 according to the INGV catalog for this area). After processing the preliminary data
181 and checking for errors, we found that the anomalies of multiple parameters were
182 more remarkable at 06:00 UTC than in other periods. Thus, all the ERA-Interim and



183 NCEP-FNL data at 06:00 UTC were selected uniformly for information extraction
184 and anomaly recognition. The daily averages and the maximum and minimum values
185 based on the data from the ground-based stations were analyzed subsequently. In
186 addition, we used the 5th and 95th percentile box plots of AOD_{532nm} each day to
187 effectively express the variations in the daily averages and maximum and minimum
188 values as a result of the differences in the daily data records [Che et al., 2014].

189 Second, the spatial distributions of the SML1, STL1, TMP2m, and PWATclm data
190 were analyzed. Considering the complex influences and possible uncertainties with
191 regard to seasons, terrain, weather, and latitude, we obtained the differential images of
192 the changed parameters (ΔP) by subtracting the 2009 daily value from the means from
193 multiple years. The result reflected a normal background, i.e.,

$$194 \quad \Delta P_t = P_t - \mu_t = P_t - \frac{1}{n} \sum_{i=1}^n P_i \quad (1)$$

195 where P_t is the daily value of a parameter in 2009 and μ_t is the corresponding daily
196 mean estimated over the years 2000-2008. The ΔP_t images on the same day in 2006
197 were applied for comparison, and the P_t for 2006 was adjusted to the means of 2000–
198 2008, except 2006.

199 **2.2 Spatio-temporal features of hydrothermal parameters**

200 **2.2.1 SML1, STL1, PWATclm, and TMP2m from assimilation datasets**

201 In the coversphere, the soil is an important layer for the transmission of mass and
202 energy from the lithosphere to the atmosphere. The hydrologic conditions and thermal
203 properties of soil could be disturbed in the seismogenic process. Our intuitive analysis
204 showed that the variation curve of the SML1 parameter of the epicenter pixel
205 appeared to decrease from March to April in 2009 and 2006 (Fig. 2.1a). However, five
206 anomalies exceeded $\mu+1.5\sigma$ before the 2009 L'Aquila main shock, with the maximum
207 anomaly occurring on March 5. In the context of the gradual seasonal increase of
208 STL1, its anomalous variation became obvious on March 30, with the value being the
209 maximum for that month (Fig. 2.1b). Although the variation amplitudes of SML1 on
210 March 29 and 31 were less than those of the former two peaks, these dates were
211 quasi-synchronous with STL1 (Fig. 2.1b). Hence, the water content and temperature



212 in the soil significantly changed at end of March 2009. Comparing the PWATclm
213 behavior in 2009 with its relative stable fluctuation in 2006, which acts as the normal
214 background, the PWATclm parameter exhibited evident peaks on March 29, 30, and
215 31; the highest value reached 27.8 kg/m^2 , which significantly exceeded $\mu+2\sigma$ (Fig.
216 2.1c). PWATclm represents the total water vapor content of the atmosphere column; in
217 this work, this parameter indicated that the moisture budgets on the surface and
218 atmosphere layer were disturbed by something abnormal. Air temperature is a direct
219 parameter related to the thermal variation in the coversphere. In our study, we also
220 found continuous anomalous peaks of TMP2m from March 29 to April 1, 2009. The
221 values in this time window exceeded $\mu+2\sigma$, except on April 1 (Fig. 2.1d). Considering
222 the reported anomalies in Table 1, we propose that the quasi-synchronous period
223 characterized by multiple parameter anomalies preceding the L'Aquila EQ is likely
224 the time window from March 29 to April 1, 2009. The details of the abnormal
225 deviation of the parameters during this time window are shown in Table 2.

226 We mapped the image series of each ΔP_i as the difference between the daily value and
227 the historical mean (μ) to investigate the spatio-temporal evolution of the investigated
228 parameters. Figure 2.2a shows that the area with an abnormal increment of ΔSML1
229 was located in the L'Aquila basin on March 29 and 31, 2009 and that the local
230 ΔSML1 reached 19.5 K to 21 K in the epicenter grid. By contrast, the spatial pattern
231 in 2006 was characterized as normal with clear homogeneity for the land in central
232 Italy (Fig. 2.2b). This result implied that the moisture on the upper soil layer of the
233 seismogenic zone abruptly increased before the main shock. Although significantly
234 anomalous ΔSML1 occurred in north Italy, such anomaly was assumed to be unrelated
235 to the L'Aquila EQ because of its large area and remote distance. Different from that
236 of ΔSML1 , the spatial anomalous field of ΔSTL1 initiated on March 29 and appeared
237 distinguishably northwest to the epicenter of the main shock on March 30, 2009 (Fig.
238 2.3a), especially along the southern segment of the *Olevano–Antrodoco* thrust (Fig. 1).
239 This abnormal pattern did not appear in 2006 (Fig. 2.3b). According to the local
240 meteorological data (Fig. 2.4), the particular spatio-temporal evolution of ΔSML1 and
241 ΔSTL1 did not result from precipitation. As changes in soil water stimulate thermal



242 change, a short delay in the change in soil temperature relative to soil moisture is
243 possible. In this work, we revealed a one-day delay between the increases in soil
244 temperature and soil moisture.

245 In the case of an abnormal variation in temperature and moisture in the soil layer,
246 hydrothermal conversion becomes increasingly significant on the surface and in the
247 atmosphere because of the wide, open space. Compared with PWATclm in almost all
248 the Italian territories and surrounding seas during the silent period, Δ PWATclm
249 showed a sudden increase on March 29, 2009; it then quickly dropped to a relatively
250 normal level on March 31, similar to the case in 2006 (Fig. 2.5). Although the
251 abnormal area of Δ PWATclm covered the entire Italy, a weaker abnormal area
252 appeared in the L'Aquila basin on March 29-31 and extended to the southeast (Fig.
253 2.5a), where it equaled Δ SML1 on March 29-31 (Fig. 2.3a). We considered the
254 possibility of the regional anomalous signal related to the seismogenic process being
255 masked by an intensive air–sea interaction in a large area on those days. Obviously,
256 both the spatial anomalies of Δ SML1 and Δ PWATclm were not controlled by
257 topographic conditions. Particularly, the normal spatial pattern of Δ TMP2m in central
258 Italy on March 28 to April 1, 2006 was slightly higher than that over the sea and
259 notably lower than that at the northern border of the Italian territory (Fig. 2.6b).
260 However, an anomalous spatial distribution of Δ TMP2m occurred on March 28 and
261 30, 2009, mainly in the intermountain area northwest of the main shock epicenter (Fig.
262 2.6a). The anomalies of the four investigated parameters were distributed mainly in
263 the L'Aquila basin or in the intermountain area northeast of the main shock epicenter
264 on March 29–31. Thus, we inferred that the regional topography (Apennine range and
265 L'Aquila basin) and tectonics (*Olevano–Antrodoto* and *Gran Sasso* thrusts) in central
266 Italy could have induced the spatial correlations of these anomalies.

267 **2.2.2 Air temperature and AOD from ground-based stations**

268 To investigate possible thermal fluctuations in situ and to support the potential
269 coupling effects of such fluctuations on the ground surface, we collected air
270 temperature and AOD data from ground-based stations. Figure 2.6 shows that the



271 daily averages and the maximum and minimum values of air temperature at the
272 L'Aquila weather station reached their peaks on March 29 and 30, 2009 (Fig. 2.7).
273 Figure 2.8 shows the AOD variations that fluctuated in three time windows of the
274 abrupt AOD increase on March 16, 30, and April 3–6, 2009. The dates in which the
275 anomalous values of air temperature and AOD were observed were consistent with
276 those for SML1, STL1, PWATclm, and TMP2m. In particular, the general AOD values
277 were less than 0.3 (Fig. 2.8a); however, the maximum AOD_{532nm} reached 0.37, 0.3,
278 and 0.46 in the three time windows, whereas the rest of the AOD_{532nm} varied around
279 0.07–0.26, which is the same as those on clear days (Fig. 2.8b). Although the Roma
280 station of AERONET is far from the epicenter and the increase in AOD was weak, the
281 observed AOD data somehow served as the reference value for L'Aquila. The
282 secondary organic aerosol (SOA) in the atmosphere is generated from the
283 photochemical reaction of gas phase precursors, such as sulfur (SO_2) and nitrogen
284 (NO_2) volatiles, as well as ozone (O_3) [Janson et al., 2001; Rickard et al., 2010],
285 whereas the photochemical production of O_3 is a result of the photo-oxidation of
286 methane (CH_4) and carbon monoxide (CO) [Dentener et al., 2006; Crutzen, 1974].
287 The increased CH_4 degassing soon after the L'Aquila EQ [Voltattorni et al., 2012;
288 Quattrocchi et al., 2011] could be hints of O_3 precursors. Hence, the anomalous
289 increments of aerosol might have been caused by the formation of SOA particulates as
290 a result of the photochemical production of O_3 from degassed CH_4 . In addition, the
291 low precipitation in March 2009 (Fig. 2.4) indicated that the weather condition during
292 this period was acceptable and that the anomalous PWATclm increment in the
293 epicenter pixel on March 29, 2009 was not caused by rainfall.

294 **2.3 Summary of the hydrothermal parameter analysis**

295 The following seismic anomalies were determined to be possible according to the
296 quasi-synchronism analysis of the abnormal changes of six hydrologic and thermal
297 parameters related to the coversphere and atmosphere and according to the spatial
298 evolution analysis of the images of the changed values. 1) The anomalies were
299 observed mainly in the L'Aquila basin southeast of the main shock epicenter ($\Delta SML1$



300 and $\Delta PWAT_{clm}$) or in the Apennines range northwest of the main shock epicenter
301 ($\Delta STL1$ and $\Delta TMP2m$). 2) The spatial migration of the hydrologic and thermal
302 changes in the upper soil layer ($\Delta SML1$ and $\Delta STL1$) could have indicated the
303 reformation and redistribution of mass and energy transmitted from the lithosphere to
304 the coversphere. 3) The spatial distribution of the increased air temperature near the
305 surface was consistent with that of the soil temperature. Hence, the thermal
306 transmission process was stable from the coversphere to the atmosphere and was
307 controlled by regional tectonics in central Italy. 4) Although the improvement in the
308 precipitable water content in the atmosphere on March 29, 2009 was masked by its
309 high values in the surrounding large area, the anomalous weak values in the L'Aquila
310 basin suggested that the water in gaseous or liquid state was influenced by the soil
311 structure (aquifers) and surface topography. Considering these findings, we propose
312 that the anomalies be interpreted as the geosphere coupling effects preceding the 2009
313 L'Aquila EQ.

314 **3. Seismic *b*-value**

315 **3.1 Data and method**

316 The EQ catalog for computing the *b*-value in this work was obtained from INGV
317 (ISIDE: <http://iside.rm.ingv.it>). This catalog covers all of Italy and its surrounding
318 regions. We analyzed the seismic data covering the periods from April 16, 2005 to
319 December 19, 2012, during which 94,953 events were recorded. Considering data
320 quality and tectonic regimes related to the 2009 L'Aquila EQ, we excluded in the
321 analysis the events that occurred at a depth of over 40 km and limited the study area to
322 the region within the 80 km radius of the epicenter of the L'Aquila main shock. Figure
323 3.1 shows the cumulative number of the analyzed data as a function of time. For the
324 curve shows a usual behavior until the end of 2009, we preferred to limit the analysis
325 to November 2009. Hence, all the succeeding analysis refers to the periods of August
326 2005 to November 2009. Referring to the changes in the slope of the plot of the
327 cumulative number of events, we identified three-staged phases of different recording
328 qualities, with P1-1 and P1-2 denoting the conditions before the 2009 L'Aquila EQ



329 and P2 denoting the conditions after the 2009 L'Aquila EQ. The details are as follows.
330 Phase P1-1: 3,552 events from April 18, 2005 to August 15, 2007;
331 Phase P1-2: 2,742 events from August 16, 2007 to April 5, 2009;
332 Phase P2: 19,782 events from April 6, 2009 to November 30, 2009;
333 In seismology, the classical Gutenberg–Richter law [Gutenberg and Richter, 1944] is
334 introduced as follows:

$$335 \quad \text{Log}N(M) = a - bM \quad (2)$$

336 where N is the number of EQs with magnitudes greater than or equal to M in a given
337 region and in a time interval; a and b are constants that describe the productivity and
338 relative size distribution of the area of concern, respectively. The study of the b -value
339 has been widely performed [Mogi, 1962; Urbancic et al., 1992; Warren and Latham,
340 1970], and its variations have been found to be caused by regional stress, material
341 properties, and temperature gradient. Using the software package ZMAP [Wiemer,
342 2001], we computed the maximum-likelihood b -values with the following Eq.(3):

$$343 \quad b = \frac{\log e}{\bar{M} - M_o + \frac{\Delta M}{2}} \quad (3)$$

344 where \bar{M} is the mean magnitude and M_o is the minimal magnitude of the given
345 sample; ΔM is the uncertainty in magnitude estimation and is usually set to 0.1. The
346 sample was considered complete down to the minimal magnitude $M_c \leq M_o$, which
347 also referred to as the magnitude of completeness [Schorlemmer and Wiemer, 2004].
348 To detect the dynamic features of the b -values, we estimated the b -values with Eq. (3)
349 in moving (partly overlapping) time windows. Generally, the sampling window
350 contains 200 seismic events, 10% of which is the sliding/overlap window (i.e., 20
351 events), b -value actually is estimated from part samples before and after each time
352 node. To visualize the spatial distribution of the b -values, all events in the study area
353 were projected onto a coordinate plane with a gridded space of 0.1° longitude by 0.1°
354 latitude. At each grid node, we sampled all the events within a radius of 20 km and
355 determined their b -values if at least $N_{\min} = 30$ events were available. Following the
356 work of De Santis et al. [2011], we also calculated the corresponding Shannon



357 entropy of the EQ related to the b -value, i.e.,

$$358 \quad H(t) = k - \log b(t) \quad (k \approx 0.072) \quad (4)$$

359 This entropic quantity allows the measurement of the level of disorder of the seismic
360 system and the missing information or uncertainty because it is universally considered
361 a fundamental macroscopic physical quantity that describes the properties of complex
362 geosystemic evolutions, such as that of the seismogenic system in the lithosphere [De
363 Santis et al., 2011].

364 **3.2 Spatio-temporal features**

365 To compare the results of De Santis et al. [2011], we also reduced the catalog by $M_c =$
366 1.4 for the time series analysis of the b -values from phase P1-2 to phase P2.
367 Following the initial stable phase in 2008, the b -value drastically decreased as the
368 main shock approaching. Figure 3.2 shows that the curve drops to the lowest point of
369 $b = 0.747$ about March 27, 2009, i.e., ~10 days before the main shock or a few days
370 before the occurrence of various thermal anomalies [Piroddi and Ranieri, 2012;
371 Piroddi et al., 2014]. Meanwhile, the entropy gradually increased to reach the peak
372 (almost 0.2, Fig. 3.2) during the same period after a long (almost) stable period and
373 then dropped one week before the main shock. Note that the exact time when the
374 peaks were reached (minimal b -value and maximal entropy) could not be detected
375 properly because ZMAP applies a moving sliding window containing 200 events for
376 computation. Hence, each curve was slightly affected by what was preceding and
377 what was following the given moment of estimation. Moreover, the b -value (or the
378 entropy) appeared to have moved rapidly to the minimum (or the maximum) on the
379 day of the main shock. This condition indicated that the regional stress was rapidly
380 released and that faults ruptured quickly close to the main shock. Both the b -value and
381 entropy were unstable after the main shock because of the aftershocks. Although we
382 used a moving window with ZMAP to calculate the b -value, and, in turn, the entropy,
383 the minimum value of b -value and the maximum value of the entropy just around the
384 time of the mainshock is real and not an artefact. Fig. 3.3 shows a smaller interval of
385 time where the entropy has been estimated in subsequent non-overlapping intervals of



386 30 seismic events each: it is clear from the observed estimates (triangles) the
387 beginning of the increase of the entropy well before the mainshock (when the entropy
388 exceeds two times the standard deviation, σ , estimated over the whole interval),
389 with maximum at around the moment of it (when the entropy exceeds even ten times
390 the standard deviation). For a better visualization of the observed general behaviour of
391 the entropy, we also draw the gray curve that defines a reasonable smoothing of the
392 entropy values: 15-point FFT (Fast Fourier Transform) before the mainshock and
393 50-point FFT smoothing after the mainshock. The different kind of smoothing is
394 related to the different rate of seismicity before and after the mainshock.

395 Then we split the catalog into two subsets in terms of their magnitudes, which were
396 lower than the estimated completeness values, i.e., $M_c = 1.2$ and $M_c = 1.0$. The spatial
397 distributions of the b -values clearly differed in the two phases before the L'Aquila EQ
398 (Fig. 3.4b and d). In phase P1-1, the b values in the L'Aquila basin and its
399 surroundings were about 1.0, which indicated a normal regional stress level because b
400 = 1.0 is a universal constant for EQs in general [Schorlemmer et al., 2005; Kagan,
401 1999]. The anomalous areas of high b -values ($b \geq 1.2$) were located in the south and
402 east of the impending L'Aquila hypocenter. By contrast, some external areas with low
403 b -values were not relevant to the seismic sequence because of existing rare
404 hypocenters (Fig. 3.4a). However, most of the relative high b -values in phase P1-1
405 changed to extremely low b -values ($b \leq 0.8$) in phase P1-2. In particular, a relatively
406 homogeneous strip of low b -values extended westward from the hypocenter and
407 crossed the southern segment of the *Olevano–Antrodoco* thrust. This effect indicated
408 the development of rock mass fracturing in the east-to-west direction, especially in the
409 south of the impending hypocenter. Coincidentally, this strip representing a high stress
410 level was consistent with the location of the strongest variation in soil temperature on
411 March 30 (Fig. 2.3a). Most of the other parts along the *Olevano–Antrodoco* and *Gran*
412 *Sasso* thrusts retained relatively high stress levels, which implied low seismicity. The
413 changed spatial patterns of the b -values from P1-1 to P1-2 indicated the adjustment of
414 the regional crust stress to a relatively high level in the seismogenic zone before the
415 L'Aquila EQ. These conditions clearly reflected the intensive seismicity and



416 significantly rapid accumulation of crustal stress occurring near the approaching
417 L'Aquila main shock hypocenter relative to other places. Figure 3.3f shows the spatial
418 distribution of the b -values after the L'Aquila EQ. Different from that happened
419 before the main shock, the low b -values occurred in the L'Aquila basin and its
420 surroundings because of the fault rupture and the subsequent aftershocks (Fig. 3.4e).
421 We also notice that the extremely low b -values (red area) covered the entire *Gran*
422 *Sasso* thrust and the footwall of the *Olevano–Antrodoco* thrust. This observation
423 indicated that the developed cracks and ruptured rocks, which resulted from the
424 normal faulting of the L'Aquila EQ, passed through the entire *Gran Sasso* thrust but
425 stopped at the footwall of the *Olevano–Antrodoco* thrust.

426 We also selected the geological section (section 1 in Fig. 3.5a) used by Piroddi et al.
427 [2014] to show the variations in the b -values with depth before the L'Aquila EQ.
428 Another section of equal length (section 2 in Fig. 3.5a), which was perpendicular to
429 section 1 crossing the epicenter, was analyzed to identify further the differences in the
430 stress distribution and rock failure between section 1 and 2. Events above depth = 20
431 km were sampled to calculate the b -values in a buffer of 20 km from the two section
432 lines (Fig. 3.5a). In Fig. 3.5b, the spatial distribution of the low b -value appeared
433 around the hypocenter and extended about 25 km to SWW of the hanging wall of the
434 *Paganica* fault along section 1. This distribution illustrated the stress accumulation at
435 a depth of 10 km, which is shown as a stripe in Fig. 3.4d. A relatively low b -value
436 zone was observed between the *Paganica* fault and the *Gran Sasso* thrust. In addition
437 to the area of the impending hypocenter, the spatial image of the b -value along section
438 2 confirmed that the low b -value zone was near the *Gran Sasso* thrust and about 20
439 km from NNW of the *Olevano–Antrodoco* thrust (Fig. 3.5b). According to this result,
440 the geo-zones of stress concentration and rock failure were related not only to the
441 normal seismogenic fault (*Paganica* fault) but also to the two large thrusts
442 (*Olevano–Antrodoco* and *Gran Sasso* thrusts) long before the L'Aquila EQ. The
443 lowest b -values centered on the hanging wall of the *Paganica* fault at depths of 5-15
444 km (Figs. 3.5b and c). As shown in the vertical imaging section, the low b -values
445 partly connected the *Paganica* fault to the *Gran Sasso* thrust. Moreover, the relations



446 between the b -values and the geological depth in the whole study area were mapped
447 to investigate the change in the stress environment of the deep earth at different
448 phases (Fig. 3.6). We observed a similar variation trend of the b -values spatially
449 related with depth before (phase P1-2) and after (phase P2) the main shock. The
450 general b -value curves at both phases initially increased from 20 km to about 12.5 km,
451 rapidly dropped to the minimum at 9.5 km, and finally increased to high values at 5
452 km, which is the lowest depth indicated in the hypocenter records. Hence, the regional
453 crust stress accumulated at a depth of about 9.5 km, whereas the stress dropped at the
454 deep and low crusts. The stress change was stable at a depth of more than 20 km in
455 the study area. Obvious curve reversals appeared twice at depths of 8–12.5 km before
456 the main shock (Fig.3.6a). Hence, heterogeneous litho-stratigraphic
457 properties affected rock failure and led to different stress states in the study area.
458 According to CROP 11 (“CROsta Profonda,” literally “Deep Crust”) studies on the
459 near-vertical seismic reflection profiles crossing central Italy, which were supported
460 by The CROP Project and were initiated in the mid-1980s with joint funding from the
461 National Research Council, AGIP Oil Company, and ENEL (National Electric
462 Company) [Di Luzio et al., 2009; Patacca et al., 2008; Tozer et al., 2002], the
463 anomalous curve reversals resulted from the litho-stratigraphic difference among the
464 Mesozoic *Gran Sasso–Genzana* unit, *Queglia* unit, *Morrone–Porrara* unit, and even
465 the western *Marsica–Meta* unit. These carbonate units mainly contain
466 shallow-platform dolomite and limestone, which were overlaid disconformably by
467 Miocene carbonate deposits and siliciclastic flysch deposits. In addition, the *Queglia*
468 unit and the deeper *Maiella* unit contain Messinian evaporite and marl. Thus, the
469 anomalous reversal of the b -value with depth could be the result of the unconformable
470 Mesozoic–Cenozoic contact; the mixed flysch, evaporate, and marl might have also
471 affected the counter-regulation of stress accumulation. Hence, we infer that 10 ± 5 km
472 was the main depth range of the seismic stress variation associated with the L’Aquila
473 EQ.

474



475 **3.3 Summary of the seismic analysis**

476 The time series analysis of the b -values in phases P1-2 and P2 shows that after late
477 December 2008, the b -value (or the entropy) rapidly went to the minimum (or the
478 maximum), specifically on March 27, 2009 (10 days before the main shock), and then
479 wildly fluctuated closely before and after the main shock. The date of occurrence of
480 the anomalously low b -value coincided with that of the reported thermal anomalies,
481 which indicated the rapid release of crust stress and fracturing of rock mass and/or
482 faults. Compared with that in phase P1-1, the image of the b -value in the latter phase
483 P1-2 showed abnormally low b -values near the impending L'Aquila hypocenter, as
484 well as a homogeneous strip of low b -values extending toward the east-to-east
485 direction and crossing the southern segment of the *Olevano–Antrodoco* thrust. After
486 the main shock, the anomalous zone of low b -values emerged in the L'Aquila basin
487 and its surroundings because of rupturing and subsequent aftershocks. The 3D spatial
488 variation of the b -value showed that the zone of low b -values obviously appeared
489 around the hanging wall of the *Paganica* fault at a depth of 5–15 km and extended to
490 20 km SWW. Similar anomalies of low b -values closely related to two large thrusts
491 were also observed in NNW of the impending hypocenter. In particular, anomalous
492 reversals of the b -values occurred twice at a depth of 8–12.5 km before the main shock,
493 thus implying that unstable stress state did relate to heterogeneous litho-stratigraphic
494 properties. The revealed spatial pattern of the b -values indicated that the space
495 evolution characteristics of the stress accumulation prior to and immediately after the
496 L'Aquila EQ reflect the spatial correlations among the L'Aquila EQ and seismic faults
497 in the central Apennines.

498 **4. Discussions**

499 As mentioned above, SML1, STL1, TMP2m, PWATclm, b -value, and even AOD have
500 quasi-synchronous time windows of anomalies. Obviously, this characteristic is not a
501 simple coincidence, but its geophysical mechanism necessitates further analysis. Here,
502 we attempt to provide a possible explanation in view of geosphere coupling.

503 **4.1 Lithosphere: deep fluid and stress**



504 The central Apennines are affected by a NE-SW striking extension and uplift. This
505 extension was responsible for the formation of intra-mountain basins, i.e., L'Aquila
506 basin, bounded by the *Gran Sasso* and *Mt. d'Ocre* ranges. During the L'Aquila
507 seismic sequence, the seismic events were focused on the upper parts of the crust with
508 a depth < 15 km; three main faults were activated by dip-slip movements in response
509 to the NE-SW extension [Di Luccio et al., 2010]. The ultimate cause of an EQ is
510 undoubtedly the crust stress exceeding the elastic limits of faults or rock mass. Crust
511 stress is indeed affected by particular geo-environmental conditions, including faults,
512 cracks, rock, and fluids, inside the lithosphere. Some studies based on the
513 measurements of the ratio of compressional velocity to shear velocity and of seismic
514 anisotropy have provided evidence that high-pressure fluid contributed to the
515 rupturing of the 2009 L'Aquila EQ [Di Luccio et al., 2010; Terakawa et al., 2010;
516 Lucente et al., 2010]. The contribution of fluids to the L'Aquila seismic sequence
517 evolution was independently confirmed by Cianchini et al. [2012] through magnetic
518 measurements from the L'Aquila geomagnetic observatory. As a result of the eastward
519 migration of the compressive front since the early Miocene, the back-arc extension
520 affected the Apennines chain, which was previously controlled by compressive
521 tectonics [Di Luccio et al., 2010]. Normal faults formed the L'Aquila basin and
522 affected the Apennines chain in the Pleistocene period [Doglioni, 1995]; moreover,
523 several works have increasingly implicated fluids and their movement in the
524 generation of the L'Aquila EQ [Di Luccio et al., 2010; Terakawa et al., 2010; Lucente
525 et al., 2010]. Both the eastward compressive and NE-SW extensive stresses could
526 have contributed to the deep fluid migration to the potential epicenter area.
527 Subsequently, seismogenic faults became weak as a result of the high pressure of pore
528 fluid and consequently reduced the stress level needed to break the rocks [Hubbert
529 and Rubey, 1959]. In particular, a proposed scenario suggested that the *Paganica* fault
530 plane initially acted as a barrier to fluid flow [Lucente et al., 2010]; hence, the fluid
531 pressures at both sides of the fault were unbalanced. The foreshock sequence,
532 especially the MI 4.0 foreshock on March 30, broke the barrier, thereby allowing
533 fluids to migrate across the fault and change the V_p/V_s ratios [Lucente et al., 2010].



534 The migrating fluids would have dilated the rock mass of the hanging wall and
535 facilitated fault movement, leading to EQ nucleation. The images of the b -values in
536 phase P1-2 (Fig. 3.4d) and along the two orthogonal sections (Fig. 3.5) clearly show
537 the spatial distribution of the intensive stress accumulation and rock failure
538 development around the impending hypocenter and the large thrust at a depth of $10 \pm$
539 5 km in the crust, which correspond to fluid migration and high pore pressure,
540 respectively.

541 At this point, we clarify basic issues on fluids. First, we discuss the composition of
542 fluids and their sources. The Apennines located at the plate boundary are
543 characterized by high heat flow and large-scale vertical expulsion, volcanoes, gas
544 vents, mud pools, geysers, and thermal springs, which are typical surface features of
545 fluid expulsion [Chiodini et al., 2004; Chiodini et al., 2011; Minissale et al., 2004].
546 Two of the largest aquifers covering the Abruzzi region are the *Velino* and *Gran Sasso*
547 aquifers (Fig. 4.1b), which consist of Meso-Cenozoic carbonate formations (limestone
548 and dolomite) of the Latium–Abruzzi platform and of platform-to-basin transitional
549 domains [Chiodini et al., 2011]. For the fluid solution, the rich groundwater breeds an
550 ideal geo-zone for gas–water–rock reactions. Fluids with CO₂-rich gases are known to
551 be involved in the EQ preparation process [Di Luccio et al., 2010; Terakawa et al.,
552 2010; Lucente et al., 2010; Chiodini et al., 2011]. Both the numerous CO₂-rich gas
553 emissions mainly from the Tyrrhenian region and the large amounts of deeply derived
554 CO₂ dissolved by the groundwater of the aquifers of the Apennines have been
555 supported by geochemical and isotopic data [Chiodini et al., 2000, 2004, 2011;
556 Minissale et al., 2004]. The melting of the crust sediments of the subducted Adriatic–
557 Ionian slab is a regional CO₂ source, and the subsequent upwelling of the mantle and
558 the carbonate rich melts would have induced the massive degassing of CO₂ on the
559 Earth’s surface [Frezzotti et al., 2009]. Thus, we conclude that the large quantities of
560 CO₂ gas in the two aquifers not only comprise a large portion of the dissolved
561 inorganic carbon derived from the Tyrrhenian mantle wedge and/or Adriatic
562 subducted slab in the deep Earth but also involve the progressive decarbonation of
563 minerals of the carbonate formations in the shallow crust.



564 Second, we explain how fluids migrate. On the one hand, Chiodini et al. [2011]
565 compared the geochemical composition of Abruzzi gas and that of 40 large gas
566 emission sites located in central Italy and found that the former becomes
567 progressively rich in radiogenic elements (^4He and ^{40}Ar) and N_2 from the volcanic
568 complexes in the west to the Apennines in the east, thereby indicating the increasing
569 residence time of the gas in the crust moving from west to east. On the other hand,
570 Minissale et al. [2004] performed a systematic analysis of published geochemical and
571 isotopic data (together with new data) from the Apennines, including thermal and cold
572 springs, gas vents (mostly CO_2), and active and fossil travertine deposits, and found
573 that meteoric water precipitating in the high eastern Apennine ranges mixes with
574 ascending eastward magmatic, metamorphic, and geothermal fluids in the highly
575 permeable Mesozoic limestone.

576 **4.2 From lithosphere to coversphere: Earth degassing**

577 Before the main shock, CO_2 -rich gases from different sources were involved in the
578 crustal circulation of fluids, and the mixed fluids could have been injected into the
579 regional groundwater system (i.e., *Velino* and *Gran Sasso* aquifers) and moved up to
580 the surface. Hence, the influx of CO_2 -rich gases can increase pore pressure and flow
581 rate. During the foreshock sequence, the development of fractures and cracks of rock
582 mass would have facilitated the flow of fluids outside the aquifers in the shallow crust,
583 which is bordered by the *Olevano–Antrodoco* and *Gran Sasso* thrusts. Meanwhile,
584 electronic charge carriers of crustal rocks in the form of peroxy defects known as
585 p-holes [Freund, 2011] could have been activated when the rock was stressed.
586 Overpressured fluid could further reduce the friction of fault planes and reactivate
587 faults. As a result of the widespread aquifers and the high permeability of carbonate
588 formations, underground fluids with CO_2 -rich gases easily migrated upward to the
589 coversphere under the accelerated stress condition. The rising of shallow underground
590 fluid alters soil physical properties (i.e., soil moisture and temperature) and thereby
591 affects different components of surface energy balance. A gas geochemical monitoring
592 conducted in a natural vent close to the L'Aquila basin observed anomalous CO_2 gas



593 flow variations in March and April 2009 [Bonfanti et al., 2012]. The intensive CO₂
594 degassing from ground measurements confirms the emission of deeply originating
595 gaseous fluids to the coversphere. The increase in greenhouse gas emission (i.e., CO₂,
596 CH₄), is an important mechanism of pre-EQ thermal anomalies. In addition, as radon
597 gas might cause air ionization and variations in humidity and latent heat exchange, the
598 anomalous Rn emanation before the L'Aquila EQ was recorded [Pulinets et al. 2010].
599 Soil gas surveys [Voltattorni et al., 2012; Quattrocchi et al., 2011] revealed CO₂ and
600 certain amounts of CH₄ and Rn as released gas phases. Hence, we propose that the
601 degassing of CO₂, CH₄ and Rn from the lithosphere to the coversphere before the
602 main shock could have resulted in the complex lithosphere–coversphere coupling
603 effect, which finally increased near-surface temperature and generated heavy TIR
604 emissions.

605 **4.3 From coversphere to atmosphere: air ionization**

606 As a transition layer from the lithosphere to the atmosphere, the coversphere affects
607 the flow and exchanges of mass and energy from the deep crust to the surface. As
608 revealed by the ESA global land cover data produced from the Medium Resolution
609 Imaging Spectrometer sensor aboard the Envisat satellite, the thermal anomalous zone
610 based on the Night Thermal Gradient (NTG) algorithm (Fig. 4.1a) was mainly
611 covered by high vegetation, i.e., broadleaved deciduous forest, with strong water
612 retention and developed root traits. Generally, high vegetation coverage represents
613 high moisture in deep soil and improves the active characteristics of surface soil,
614 including organic matter contents, which promote fluid concentration and movement
615 through preferential flow and root absorption [Chai et al., 2008; Millikin et al., 1999]
616 Hence, we propose that high vegetation in central Italy facilitated the upward
617 migration of CO₂-rich fluids inside the coversphere before the 2009 L'Aquila EQ. We
618 also suggest that this upward migration of CO₂-rich fluids generated heavy thermal
619 radiations because surface temperature rise results from possible greenhouse effects
620 together with latent heat release stimulated by the decay of radon and/or the activation
621 of P-holes.



622 Air ionization is a fundamental factor of energy balance in the lower atmosphere.
623 When underground gases are released on the surface, the air composition of the lower
624 atmosphere must change. The leaked CO₂ and CH₄ gases on the surface can serve as
625 radon carriers, and α -particles emitted by a certain amount of decayed radon can
626 further motivate the air ionization process [Pulinets and Ouzounov, 2011]. In addition,
627 the activated p-hole outflow leads to air ionization at the ground–air interface [Freund,
628 2011]. Hence, both radon emanation and P-hole activation processes could have
629 contributed to the air ionization and resulting ion hydration before the 2009 L’Aquila
630 EQ. The direct results of ion hydration are humidity change and latent heat release. In
631 turn, increased latent heat changes the content of water vapor. In this work, the local
632 greenhouse effect and latent heat release jointly resulted in the increase in air
633 temperature, and TIR anomalies (i.e., NTG) were observed by satellite sensors before
634 the 2009 L’Aquila EQ. Ion hydration in the air requires particulate matter as water
635 condensation nucleus after air ionization; hence, aerosol particle injection (AOD
636 increase) is theoretically necessary [Qin et al., 2014b].

637 Although rock failure developed mainly in the hypocenter area and related to normal
638 faulting, the *b*-value features of the thrusts in the wing of the *Paganica* fault indicate
639 that NTG thermal anomalies are indeed related to compressive stress. Some key
640 matters, such as CO₂, CH₄, and radon, can be enriched at a shallow depth and
641 transported to the surface along the two seismic faults to finally cause regional
642 thermal anomalies. The hypocenter area is bounded by two intersecting thrusts, with
643 the *Olevano–Antrodoco* thrust being the main one. The experimental TIR observations
644 on the fracturing of loaded intersected faults revealed the close relationship between
645 the changed TIR radiation and the geometrical structure of intersected faults, with
646 abnormal TIR spots usually occurring along the main fault [Wu et al., 2004, 2006]. In
647 addition, two separate zones of surface NTG anomalies (Fig. 4.1a) could have
648 different modes from deeper thermal sources.

649 Therefore, a particular LCA coupling mode is proposed to interpret the
650 comprehensive geophysical mechanisms of multi-parameter anomalies associated
651 with the 2009 L’Aquila EQ. Before the main shock, the deep CO₂-rich fluids changed



652 the geo-environment in the lithosphere, including the geophysical properties of rock
653 mass, the chemical composition of groundwater, and fault activity. Thus, the resulting
654 intensive crust stress varied in the specific area, particularly in the southern segment
655 of the *Olevano–Antrodoco* thrust. Forced by the resulting intensive stress and driven
656 by high-pressure fluids, abnormal gas matters (including CO₂, CH₄, and Rn) and heat
657 energy moved up to the coversphere and altered the water content and temperature in
658 the soil layer (i.e., SML1 and STL1). Furthermore, soil and vegetation facilitated the
659 upward migration of CO₂-rich fluids to the atmosphere. In general, a chain of LCA
660 coupling effects related to the L’Aquila EQ occurred as 1) the upwelling of
661 underground fluids increased the soil temperature (STL1) and SML1; 2) the decay of
662 radon and the activation of P-holes led to air ionization; 3) the triggering of air
663 ionization and subsequent ion hydration were promoted by aerosol particle injection;
664 4) a series variation occurred in water and heat, including a drop in atmospheric
665 relative humidity, latent heat release, and change in water vapor (i.e., PWAT_{clm}); 5)
666 air temperature increased (i.e., TMP_{2m}); and 6) TIR anomalies (i.e., NTG) were
667 observed from the satellite sensors.

668 5. Conclusions

669 The anomalies of hydrothermal parameters in the coversphere and atmosphere before
670 the 2009 L’Aquila EQ appeared in significant quasi-synchronous time windows on
671 March 29-31, 2009 (three days). The spatial patterns of these anomalies were
672 controlled by the seismogenic tectonics and local topography. The temperature
673 variation of the soil and the near-surface atmosphere, which was mainly distributed in
674 the intermountain northwest of the main shock epicenter, indicated that the thermal
675 anomalies were geo-related to the large thrusts outside the rupturing zone. Moreover,
676 the zones of the most intensive soil and air temperature anomalies were consistent
677 with that of NTG from the satellite and with the increased *b*-value in phase P1-2. The
678 results related to the hydrographic and thermal anomalies in the coversphere and
679 atmosphere compensate for the deficiency in current interpretations on the LCA
680 coupling of the 2009 L’Aquila EQ. The supplemental temporal analysis of air



681 temperature and AOD further proved the dates of thermal anomalies and supported
682 the coversphere-atmosphere coupling effects.

683 As a parameter of stress meter, the *b*-value should be applied to EQ anomaly
684 recognition and the analysis of geosphere coupling effects to logically and spatially
685 link multiple observations on the coversphere and atmosphere with that on the
686 lithosphere. In this study, we deduced from the dynamic variation of the *b*-values that
687 the regional stress had started to rapidly accumulate in late December 2008 and soon
688 entered the nucleation stage. The end of March, 2009 was possibly a critical time
689 node of stress transition. The 3D variation features of the *b*-values revealed that the
690 regional crust stress accumulated to a relatively high level from phase P1-1 to phase
691 P2-2 in the hypocenter area before the main shock. The *b*-values notably decreased
692 after the main shock because of the aftershock sequence. Furthermore, the relation
693 between the *b*-values and the hypocenter depth indicated that the shallow crust with a
694 depth of less than 10 km was the main geo-layer characterized by a high stress level,
695 especially near the *Paganica* fault and the southern segment of the *Olevano–*
696 *Antrodoco* thrust. The depth of 10 ± 5 km was considered as the main depth range of
697 the crustal stress transition related to the 2009 L'Aquila EQ.

698 Regional/local tectonics, lithology, hydrogeology, geochemistry, and land cover have
699 great influence and/or control over the generation and spatio-temporal evolution of
700 multiple anomalies before a tectonic EQ. CO₂-rich underground fluids played a vital
701 role in the coupling processes from the lithosphere to the coversphere in the 2009
702 L'Aquila EQ because their characteristics benefitted the migration of mass and energy
703 from the lithosphere to the coversphere. Hence, to clearly understand the phenomena
704 and mechanisms of anomalous signals related to tectonic EQs, we need to pay close
705 attention to local geological, hydrogeological, and geographical environments. The
706 coversphere is a key part of geospheres and has a major effect on the production and
707 transmission of seismic signals as well as anomalies. Knowledge of the coversphere is
708 extremely important in studying the mechanism and physical process of LCA or LCAI
709 coupling before tectonic EQs. Moreover, certain particular matters in the deep Earth,
710 such as deep-originated fluid, including water and gases, should be investigated to



711 analyze and understand the observed pre-EQ anomalies.

712 **Acknowledgements**

713 This work is supported by the National Basic Research Program of China (973
714 Program) (Grant No.2011CB707102) of the China Ministry of Science and the
715 Technology, and some parts of this work has been performed under the auspices of the
716 SAFE (Swarm for Earthquake study) ESA-funded Project. The hydrothermal
717 parameters were obtained freely by ERA-Interim (<http://apps.ecmwf.int/datasets/data>)
718 and NCEP-FNL (<http://rda.ucar.edu/datasets>). The AOD data were obtained freely
719 from NASA AORNET (<http://aeronet.gsfc.nasa.gov/>). The *b*-value data were
720 generated by Italy seismic catalog and obtained by INGV (ISIDE:
721 <http://iside.rm.ingv.it>). The seismic and weather data about L'Aquila have been
722 downloaded from two open-access (upon free registration) websites: The seismic
723 data from seismic catalog ISIDE (<http://iside.rm.ingv.it/>) maintained by the Istituto
724 Nazionale di Geofisica e Vulcanologia (INGV), Italy, while the wheather data have
725 been taken from <http://cetemps.aquila.infn.it/> maintained by CETEMPS, Italy.

726 **References**

- 727 Akhoondzadeh, M., M. Parrot, and M. R. Saradjian (2010). Electron and ion density
728 variations before strong earthquakes ($M > 6.0$) using DEMETER and GPS data. *Nat.*
729 *Hazards Earth Syst. Sci.*, 10, 7-18, doi:10.5194/nhess-10-7-2010.
- 730 Benoit, M. H., M. Torpey, K. Liszewski, V. Levin, and J. Park (2011). P and S wave
731 upper mantle seismic velocity structure beneath the northern Apennines: New
732 evidence for the end of subduction. *Geochem. Geophys. Geosys.*, 12(6), 1-19,
733 doi:10.1029/2010GC003428.
- 734 Biagi, P. F., L. Castellana, T. Maggipinto, D. Loiacono, L. Schiavulli, T. Ligonzo, M.
735 Fiore, E. Suciù, and A. Ermini (2009). A pre seismic radio anomaly revealed in the
736 area where the Abruzzo earthquake ($M=6.3$) occurred on 6 April 2009. *Nat.*
737 *Hazards Earth Syst. Sci.*, 9, 1551-1556, doi:10.5194/nhess-9-1551-2009.
- 738 Bonfanti, P., N. Genzano, J. Heinicke, F. Italiano, G. Martinelli, N. Pergola, L. Telesca,
739 and V. Tramutoli (2012). Evidence of CO₂-gas emission variations in the central
740 Apennines (Italy) during the L'Aquila seismic sequence (March-April 2009).



- 741 *Boll.Geof.Teor.Appl.*, 53, 147-168, doi:10.4430/bgta0043.
- 742 Chai, W., G. X. Wang, Y. S. Li, and H. C. Hu (2008). Response of soil moisture under
743 different vegetation coverage to precipitation in the headwaters of the Yangtze
744 river. *J. Glaciol. Geocryol. (in Chinese)*, 30(2), 329-337.
- 745 Che, H., X. Xia, J. Zhu, Z. Li, O. Dubovik, B. Holben, P. Goloub, H. Chen, V. Estelles,
746 E. Cuevas-Agullo, L. Blarel, H. Wang, H. Zhao, X. Zhang, Y. Wang, J. Sun, R. Tao,
747 X. Zhang and G. Shi (2014). Column aerosol optical properties and aerosol
748 radiative forcing during a serious haze-fog month over North China Plain in 2013
749 based on ground-based sunphotometer measurements. *Atmos.Chem.Phys.* 14,
750 2125-2138, doi:10.5194/acp-14-2125-2014.
- 751 Cianchini, G., A. De Santis, D. R. Barraclough, L. X. Wu, and K. Qin (2012).
752 Magnetic transfer function entropy and the 2009 Mw = 6.3 L'Aquila earthquake
753 (Central Italy). *Nonlin. Processes Geophys.*, 19, 401-409, doi:10.5194/npg-19-401
754 -2012.
- 755 Cicerone, R. D., J. E. Ebel, and J. Britton (2009). A systematic compilation of
756 earthquake precursors. *Tectonophysics.*, 476, 371-396, doi:10.1016/j.tecto.2009.06.
757 008.
- 758 Chiarabba, C., S. Bagh, I. Bianchi, P. De Gori and M. Barchi (2010). Deep structural
759 heterogeneities and the tectonic evolution of the Abruzzi region (Central
760 Apennines, Italy) revealed by microseismicity, seismic tomography, and
761 teleseismic receiver functions. *Earth Planet. Sc. Lett.* 295, 462-476, doi:10.1016/
762 j.epsl.2010.04.028.
- 763 Chiodini, G., C. Cardellini, A. Amato, E. Boschi, S. Caliro, F. Frondini, and G.
764 Ventura (2004). Carbon dioxide Earth degassing and seismogenesis in central and
765 southern Italy. *Geophys.Res.Lett.*, 31, L07615, doi:10.1029/2004GL019480.
- 766 Chiodini, G., F. Frondini, C. Cardellini, F. Parello, and L. Peruzzi (2000). Rate of
767 diffuse carbon dioxide Earth degassing estimated from carbon balance of regional
768 aquifers: The case of central Apennine, Italy. *J.Geophys.Res.*, 105(B4), 8423-8434,
769 doi:10.1029/1999JB900355.
- 770 Chiodini, G., S. Caliro, C. Cardellini, F. Frondini, S. Inguaggiato, and F. Matteucci



- 771 (2011). Geochemical evidence for and characterization of CO₂ rich gas sources in
772 the epicentral area of the Abruzzo 2009 earthquakes. *Earth Planet. Sci. Lett.*, 304,
773 389-398, doi:10.1016/j.epsl.2011.02.016.
- 774 Crutzen, P. J. (1974). Photochemical reactions initiated by and influencing ozone in
775 unpolluted tropospheric air. *Tellus*. 26, 47-57, doi:10.1111/j.2153-3490.1974.tb0
776 1951.x.
- 777 De Santis, A., G. Cianchini, P. Favali, L. Beranzoli, and E. Boschi (2011). The
778 Gutenberg–Richter Law and Entropy of Earthquakes: Two Case Studies in Central
779 Italy. *B.Seismol.Soc.Am.*, 101(3), 1386-1395, doi:10.1785/0120090390.
- 780 Dentener, F., S. Kinne, T. Bond, O. Boucher, J. Cofala, S. Generoso, P. Ginoux, S.
781 Gong, J. J. Hoelzemann, A. Ito, L. Marelli, J. E. Penner, J. P. Putaud, C. Textor, M.
782 Schulz, G. R. van der Werf and J. Wilson (2006). Emissions of primary aerosol and
783 precursor gases in the years 2000 and 1750 prescribed data-sets for AeroCom.
784 *Atmos. Chem. Phys.* 6, 4321-4344, doi:10.5194/acp-6-4321-2006.
- 785 Dey, S., and R. P. Singh (2003). Surface latent heat flux as an earthquake precursor.
786 *Nat. Hazards Earth Syst.Sci.*, 3 (6), 749-755, doi:10.5194/nhess-3-749-2003.
- 787 Di Luccio, F., G. Ventura, R. Di Giovambattista, A. Piscini, and F. R. Cinti (2010).
788 Normal faults and thrusts reactivated by deep fluids: The 6 April 2009 Mw 6.3
789 L'Aquila earthquake, central Italy. *J.Geophys.Res.*, 115, B06315, doi:10.1029/
790 2009JB007190.
- 791 Di Luzio, E., G. Mele, M. M. Tiberti, G. P. Cavinato, and M. Parotto (2009). Moho
792 deepening and shallow upper crustal delamination beneath the central Apennines.
793 *Earth Planet. Sci. Lett.*, 280, 1-12, doi: 10.1016/j.epsl.2008.09.018.
- 794 Doglioni, C. (1995). Geological remarks on the relationships between extension and
795 562 convergent geodynamic settings. *Tectonophysics*. 252, 253-268, doi:10.1016/
796 0040-1951(95)00087-9.
- 797 Eftaxias, K., G. Balasis, Y. Contoyiannis, C. Papadimitriou, M. Kalimeri, L.
798 Athanasopoulou, S. Nikolopoulos, J. Kopanas, G. Antonopoulos, and C. Nomicos
799 (2010). Unfolding the procedure of characterizing recorded ultralow frequency,
800 kHz and MHz electromagnetic anomalies prior to the L'Aquila earthquake as



- 801 pre-seismic ones - Part 2. *Nat. Hazards Earth Syst. Sci.*, 10, 275-294, doi:10.5194/
802 nhess-10-275-2010.
- 803 Freund, F. (2011). Pre-earthquake signals: Underlying physical processes. *J. Asian*
804 *Earth Sci.*, 41, 383-400, doi:10.1016/j.jseae.2010.03.009.
- 805 Frezzotti, M. L., A. Peccerillo, and G. Panza (2009). Carbonate metasomatism and
806 CO₂ lithosphere–asthenosphere degassing beneath the Western Mediterranean: an
807 integrated model arising from petrological and geophysical data. *Chem. Geol.*
808 262,108-120, doi:10.1016/j.chemgeo.2009.02.015.
- 809 Galadini, F., and P. Galli (2000). Active Tectonics in the Central Apennines (Italy)
810 -Input Data for Seismic Hazard Assessment. *Nat.Hazards.*, 22(3), 225-268, doi:
811 10.1023/A:1008149531980.
- 812 Geng, N. G., P. Yu, M. D. Deng, C. Y. Cui, and Z. L. Luo (1998). The simulated
813 experimental studies on cause of thermal infrared precursor of earthquake.
814 *Earthquake* (in Chinese), 18(1):83-88.
- 815 Genzano, N., C. Aliano, R. Corrado, C. Filizzola, M. Lisi, G. Mazzeo, R. Paciello, N.
816 Pergola, and V. Tramutoli (2009). RST analysis of MSG-SEVIRI TIR radiances at
817 the time of the Abruzzo 6 April 2009 earthquake. *Nat. Hazards Earth Syst. Sci.*, 9,
818 2073-2084, doi:10.5194/nhess-9-2073-2009.
- 819 Gregori, G. P., M. Poscolieri, G. Paparo, S. De Simone, C. Rafanelli, and G. Ventrice
820 (2010). “Storms of crustal stress” and AE earthquake precursors. *Nat. Hazards*
821 *Earth Syst. Sci.*, 10, 319-337, doi:10.5194/nhess-10-319-2010.
- 822 Gulia, L., and S. Wiemer (2010). The influence of tectonic regimes on the earthquake
823 size distribution: A case study for Italy. *Geophys.Res.Lett.*, 37, L10305,
824 doi:10.1029/2010GL043066.
- 825 Gutenberg, B., and C. F. Richter (1944). Frequency of earthquake in California.
826 *B.Seismol.Soc.Am.*, 34,185-188.
- 827 Hubbert, K. M., and Rubey, W. W. (1959). Role of Fluid pressure in mechanics of
828 overthrust faulting. *Geol.Soc.Am. Bull.*, 70, 115-166, doi:10.1130/0016-7606(1959)
829 70[115:ROFPIM]2.0.CO;2.
- 830 Janson, R., K. Rosman, A. Karlsson, and C. Hansson (2001). Biogenic emissions and



- 831 gaseous precursors to forest aerosols. *Tellus*. 53(B), 423-440, doi:10.1034/j.1600-
832 0889.2001.530408.x.
- 833 Jing, F., X. H. Shen, C. L. Kang, X. Pan, and K. Sun (2012). Variation of outgoing
834 longwave radiation around the time of New Zealand earthquake M7.1, 2010. *Adv.*
835 *Earth Sci. (in Chinese)*, 27(9), 979-986.
- 836 Jordan, T. H., Y. T. Chen, P. Gasparini, R. Madariaga, I. Main, W. Marzocchi, G.
837 Papadopoulos, G. Sobolev, K. Yamaoka, and J. Zschau (2011). Operational
838 Earthquake Forecasting: State of knowledge and guidelines for utilization.
839 *Ann.Geophys.*, 54(4), 315-391, doi: 10.4401/ag-5350.
- 840 Kagan, Y. (1999). Universality of the seismic moment-frequency relation. *PAGEOP*,
841 155, 537-574, doi:10.1007/s000240050277.
- 842 Liperovsky, V. A., C. V. Meister, E. V. Liperovskaya, and V. V. Bogdanov (2008a). On
843 the generation of electric field and infrared radiation in aerosol clouds due to radon
844 emanation in the atmosphere before earthquakes. *Nat. Hazards Earth Syst. Sci.*, 8,
845 1199-1205, doi:10.5194/nhess-8-1199-2008.
- 846 Liperovsky, V. A., O. A. Pokhotelov, C. V. Meister, and E. V. Liperovskaya (2008b).
847 Physical models of coupling in the lithosphere–atmosphere–ionosphere system
848 before earthquakes. *Geomagn.Aeronomy.*, 48 (6), 795-806, doi:10.1134/S001679
849 3208060133.
- 850 Lisi, M., C. Filizzola, N. Genzano, C. S. L. Grimaldi, T. Lacava, F. Marchese, G.
851 Mazzeo, N. Pergola, and V. Tramutoli (2010). A study on the Abruzzo 6 April
852 2009 earthquake by applying the RST approach to 15 years of AVHRR TIR
853 observations. *Nat. Hazards Earth Syst. Sci.*, 10, 395-406, doi:10.5194/nhess-10-
854 395-2010.
- 855 Lucente, F. P., P. De Gori, L. Margheriti, D. Piccinini, M. Di Bona, C. Chiarabba, and
856 N. P. Agostinetti (2010). Temporal variation of seismic velocity and anisotropy
857 before the 2009 Mw 6.3 L'Aquila earthquake, Italy. *Geology*, 38 (11), 1015-1018,
858 doi:10.1130/G31463.1.
- 859 Millikin, C. S., and C. S. Bledsoe (1999). Biomass and distribution of fine and coarse
860 roots from blue oak (*Quercus douglasii*) trees in the northern Sierra Nevada



- 861 foothills of California. *Plant.Soil.*, 214, 27-81, doi:10.1023/A:1004653932675.
- 862 Minissale, A. (2004). Origin, transport and discharge of CO₂ in central Italy. *Earth*
863 *Sci.Rev.*, 66, 89-141, doi:10.1016/j.earscirev.2003.09.001.
- 864 Mogi, K. (1962). Magnitude-Frequency relation for elastic shocks accompanying
865 fractures of various materials and some related problems in earthquakes.
866 *B.Earthq.Res.Inst.*, 40, 831-853.
- 867 Montone, P., M. T. Mariucci, and S. Pondrelli (2012). The Italian present-day stress
868 map. *Geophys. J. Int.*, 189, 705-716, doi:10.1111/j.1365-246X.2012.05391.x.
- 869 Montone, P., M. T. Mariucci, S. Pondrelli, and A. Amato (2004). An improved stress
870 map for Italy and surrounding regions (central Mediterranean). *J.Geophys.Res.*,
871 109, B10410, doi:10.1029/2003JB002703.
- 872 Ouzounov, D., D. F. Liu, C. L. Kang, G. Cervone, M. Kafatos, and P. Taylor (2007).
873 Outgoing longwave radiation variability from IR satellite data prior to major
874 earthquakes. *Tectonophysics*, 431, 211-220, doi:10.1016/j.tecto.2006.05.042.
- 875 Papadopoulos, G. A., M. Charalampakis, A. Fokaefs, and G. Minadakis (2010).
876 Strong foreshock signal preceding the L'Aquila (Italy) earthquake (Mw 6.3) of 6
877 April 2009. *Nat. Hazards Earth Syst. Sci.*, 10, 19-24, doi:10.5194/nhess-10-19-
878 2010.
- 879 Patacca, E., P. Scandone, E. Di Luzio, G. P. Cavinato, and M. Parotto (2008).
880 Structural architecture of the central Apennines: Interpretation of the CROP 11
881 seismic profile from the Adriatic coast to the orographic divide. *Tectonics*, 27(3),
882 620-628, doi:10.1029/2005TC001917.
- 883 Piroddi, L., and G. Ranieri (2012). Night thermal gradient: a new potential tool for
884 earthquake precursors studies. an application to the seismic area of L'Aquila
885 (central Italy). *IEEE J. STARS.*, 5(1), 307-312, doi:10.1109/JSTARS.2011.
886 2177962.
- 887 Piroddi, L., G. Ranieri, F. Freund, and A. Trogu (2014). Geology, tectonics and
888 topography underlined by L'Aquila earthquake TIR precursors. *Geophys.J.Int.*,
889 197, 1532-1536, doi:10.1093/gji/ggu123.
- 890 Plastino, W., P. P. Povinec, G. D. Luca, C. Doglioni, S. Nisi, L. Ioannucci, M. Balata,



- 891 M. Laubenstein, F. Bella, and E. Coccia (2010). Uranium groundwater anomalies
892 and L'Aquila earthquake, 6th April 2009 (Italy). *J.Environ.Radioactiv.*, 101(1),
893 45-50, doi:10.1016/j.jenvrad.2009.08.009.
- 894 Pulinet, S. A. (2012). Low-latitude atmosphere-ionosphere effects initiated by strong
895 earthquakes preparation process. *Int.J.Geophys.*, 14, 1-14, doi:10.1155/2012/
896 131842.
- 897 Pulinet, S. A., and D. Ozounov (2011). Lithosphere-Atmosphere-Ionosphere
898 Coupling (LAIC) model-An unified concept for earthquake precursors validation.
899 *J. Asian Earth Sci.*, 41, 371-382, doi: 10.1016/j.jseaes.2010.03.005.
- 900 Pulinet, S. A., D. Ozounov, G. Giuliani, L. Ciralo, and P. Taylor (2010). Atmosphere
901 awakening prior to Abruzzo, Italy, M6.3 Earthquake of April 6, 2009 revealed by
902 joined satellite and ground observations. *Geophysical Research Abstracts*, 12,
903 EGU2010-12869.
- 904 Pulinet, S. A., D. Ozounov, L. Ciralo, R. Singh, G. Cervone, A. Leyva, M.
905 Dunajacka, A. V. Karelin, K. A. Boyarchunk, and A. Kotsarenko (2006). Thermal,
906 atmospheric and ionospheric anomalies around the time of the Colima M7.8
907 earthquake of 21 January 2003. *Ann.Geophys.*, 24, 835-849, doi:10.5194/angeo-
908 24-835-2006.
- 909 Qin, K., L. X. Wu, A. De Santis, J. Meng, W. Y. Ma, and G. Cianchini (2012).
910 Quasi-synchronous multi-parameter anomalies associated with the 2010-2011 New
911 Zealand earthquake sequence. *Nat. Hazards Earth Syst. Sci.*, 12, 1059-1072, doi:
912 10.5194/nhess-12-1059-2012.
- 913 Qin, K., L. Wu, X. Y. Ouyuang, X. H. Shen, and S. Zheng (2014a). Surface latent heat
914 flux anomalies quasi-synchronous with ionospheric disturbances before the 2007
915 Pu'er earthquake in China. *Adv. Space Res.*, 53(2), 266-271, doi:10.1016/j.asr.
916 2013.11.004.
- 917 Qin, K., L. Wu, S. Zheng, Y. Bai, and X. Lv (2014b). Is there an abnormal
918 enhancement of atmospheric aerosol before the 2008 Wenchuan earthquake? *Adv.*
919 *Space Res.*, 54, 1029-1034, doi:10.1016/j.asr.2014.04.025.
- 920 Qin, K., L. Wu, S. Zheng, and S. Liu (2013). A Deviation-Time-Space-Thermal



- 921 (DTS-T) Method for Global Earth Observation System of Systems
922 (GEOSS)-Based Earthquake Anomaly Recognition: Criteria and
923 Quantify Indices. *Remote Sens.*, 5(10), 5143-5151, doi:10.3390/rs5105143.
- 924 Quattrocchi, F., G. Galli, A. Gasparini, L. Magno, L. Pizzino, A. Sciarra, and N.
925 Voltattorni (2011). Very slightly anomalous leakage of CO₂, CH₄ and radon along
926 the main activated faults of the strong L'Aquila earthquake (Magnitude 6.3, Italy).
927 Implications for risk assessment monitoring tools & public acceptance of CO₂ and
928 CH₄ underground storage. *Energy Procedia*, 4, 4067-4075, doi:10.1016/j.egypro.
929 2011.02.349.
- 930 Rickard, A. R., K. P. Wyche, A. Metzger, P. S. Monks, A. M. Ellis, J. Dommen, U.
931 Baltensperger, M. E. Jenkin, and M. J. Pilling (2010). Gas phase precursors to
932 anthropogenic secondary organic aerosol: Using the Master Chemical Mechanism
933 to probe detailed observations of 1,3,5-trimethylbenzene photo-oxidation. *Atmos.*
934 *Environ.*, 44, 5423-5433, doi:10.1016/j.atmosenv.2009.09.043.
- 935 Rozhnoi, A., M. Solovieva, O. Molchanov, K. Schwingenschuh, M. Boudjada, P. F.
936 Biagi, T. Maggipinto, L. Castellana, A. Ermini, and M. Hayakawa (2009).
937 Anomalies in VLF radio signals prior the Abruzzo earthquake (M=6.3) on 6 April
938 2009. *Nat. Hazards Earth Syst. Sci.*, 9, 1727-1732, doi:10.5194/nhess-9-1727-
939 2009.
- 940 Saraf, A. K., and S. Choudhury (2004). Satellite detects surface thermal anomalies
941 associated with the Algerian earthquakes of May 2003. *Int. J. Remote Sens.*, 26,
942 2705-2713, doi:10.1080/01431160310001642359.
- 943 Schorlemmer, D., and S. Wiemer (2004). Earthquake statistics at Parkfield: 1.
944 Stationarity of b values. *J. Geophys. Res.*, 109(B12), 159-163, doi:10.1029/2004
945 JB003234.
- 946 Schorlemmer, D., and S. Wiemer (2005). Earth science: Microseismicity data forecast
947 rupture area. *Nature*, 434, 1086, doi:10.1038/4341086a.
- 948 Schorlemmer, D., S. Wiemer, and M. Wyss (2005). Variations in earthquake-size
949 distribution across different stress regimes. *Nature*, 437(22), 539-542, doi:10.1038
950 /nature04094.



- 951 Terakawa, T., A. Zoporowski, B. Galvan, and S. A. Miller (2010). High-pressure fluid
952 at hypocentral depths in the L'Aquila region inferred from earthquake focal
953 mechanisms. *Geology*, 38 (11), 995-998, doi:10.1130/G31457.1.
- 954 Tormann, T., B. Enescu, J. Woessner, and S. Wiemer (2015). Randomness of
955 megathrust earthquakes implied by rapid stress recovery after the Japan earthquake.
956 *Nat.Geosci.*, 8, 152-158, doi:10.1038/ngeo2343.
- 957 Tormann, T., S. Wiemer, and A. Mignan (2014). Systematic survey of high-resolution
958 b value imaging along Californian faults: Inference on asperities.
959 *J.Geophys.Res.Solid Earth*, 119, 2029-2054, doi:10.1002/2014JB011269.
- 960 Tozer, R. S. J., R. W. H. Butler, and S. Corrado (2002). Comparing thin- and
961 thick-skinned thrust tectonic models of the Central Apennines, Italy. *EGU Stephan
962 Mueller Special Publication Series*, 1, 181-194, doi:10.5194/smsps-1-181-2002.
- 963 Tronin, A. A., M. Hayakawa, and O.A. Molchanov (2002). Thermal IR satellite data
964 application for earthquake research in Japan and China. *J.Geodyn.*, 33, 519-534,
965 doi:10.1016/S0264-3707(02)00013-3.
- 966 Tsolis, G. S., and T. D. Xenos (2010). A qualitative study of the seismo-ionospheric
967 precursors prior to the 6 April 2009 earthquake in L'Aquila, Italy. *Nat. Hazards
968 Earth Syst. Sci.*, 10, 133-137, doi:10.5194/nhess-10-133-2010.
- 969 Urbancic, T. I., C. I. Trifu, J. M. Long, and R. P. Young (1992). Space-time
970 correlations of b values with stress release. *PAGEOP.*, 139, 449-462, doi:10.1007/
971 BF00879946.
- 972 USGS (2009). [http://earthquake.usgs.gov/earthquakes/eqinthenews/2009/us2009fcf
973 /# summ-ary](http://earthquake.usgs.gov/earthquakes/eqinthenews/2009/us2009fcf/#summ-ary).
- 974 Voltattorni, N., F. Quattrocchi, A. Gasparini, and A. Sciarra (2012). Soil gas degassing
975 during the 2009 L'Aquila earthquake: study of the seismotectonic and fluid
976 geochemistry relation. *Ital. J. Geosci. (Boll. Soc. Geol. It.)*, 131(3), 440-447,
977 doi:10.3301/IJG.2012.19.
- 978 Warren, N. W., and G. V. Latham (1970). An experimental study of thermally induced
979 microfracturing and its relation to volcanic seismicity. *J.Geophys.Res.*, 75,
980 4455-4464, doi:10.1029/JB075i023p04455.



- 981 Wiemer, S. (2001). A software package to analyze seismicity: ZMAP.
982 *Seismol.Res.Lett.*, 72 (3), 373-382, doi:10.1785/gssrl.72.3.373.
- 983 Wiemer, S., and M. Wyss (2002). Mapping spatial variability of the
984 frequency-magnitude distribution of earthquakes. *Adv. Geophys.*, 45, 259-302,
985 doi:10.1016/S0065-2687(02)80007-3.
- 986 Wu, L. X., K. Qin, and S. J. Liu (2012). GEOSS-Based Thermal Parameters Analysis
987 for Earthquake Anomaly Recognition. *P.IEEE.*, 100(10), 2891-2907, doi:10.1109/
988 JPROC.2012.2184789.
- 989 Wu, L. X., S. J. Liu, X. H. Xu, Y. H. Wu, and Y. Q. Li (2004). Remote sensing-rock
990 mechanics— laws of thermal infrared radiation and acoustic emission from friction
991 sliding intersected faults and its meanings for tectonic earthquake omens. *Chin. J.*
992 *of Rock Mech. & Engin (in Chinese).*, 23(3), 401-407.
- 993 Wu, L. X., S. J. Liu, Y. H. Wu, and C. Y. Wang (2006). Precursors for rock fracturing
994 and failure-Part I: IRR image abnormalities. *Int J Rock Mech Mining Sci.*, 43(3),
995 473-482, doi:10.1016/j.ijrmms.2005.09.002.
- 996 Wyss, M., and S. Wiemer (2000). Change in the Probability for Earthquakes in
997 Southern California Due to the Landers Magnitude 7.3 Earthquake. *Science*, 290,
998 1334-1338, doi:10.1126/science.290.5495.1334.
- 999 Zheng, S., L. X. Wu, and K. Qin (2014). Multiple parameters anomalies for verifying
1000 the geosystem spheres coupling effect: a case study of the 2010 Ms7.1 Yushu
1001 earthquake in China. *Ann.Geophys.*, 57(4), S0434, doi:10.4401/ag-6508.
- 1002
- 1003
- 1004
- 1005
- 1006
- 1007
- 1008



1009 **Table 1** Reported multiple parameter anomalies associated with the Mw 6.3 2009 L'Aquila EQ

<i>Parameters</i>	<i>Date of alternative anomalies</i>	<i>Geospheres</i>	<i>Reference</i>
Acoustic Emission	from 4 th to 5 th March	Lithosphere	Gregori et al., 2010
Seismicity rate	from 27 th March to 6 th April	Lithosphere	Papadopoulos et al., 2010
<i>b</i> -value	27 th March	Lithosphere	Papadopoulos et al., 2010
Entropy of <i>b</i> -value	from 31 st March to 6 th April	Lithosphere	De Santis et al., 2011
LF radio wave	from 31 st March to 1 st April	Lithosphere	Biagi et al., 2009
ULF magnetic	from 29 th March to 3 rd April	Lithosphere	Eftaxias et al., 2009
VLF electric	started on 1 st April	Lithosphere	Rozhnoi et al., 2009
CO ₂ flow-rate	started on 31 st March	Coversphere	Bonfanti et al., 2012
Radon	started on 30 th March	Coversphere	Pulinets et al., 2010
Uranium groundwater	started at beginning of March	Coversphere	Plastino et al., 2009
Land surface temperature	started on 29 th March	Coversphere	Piroddi and Ranieri, 2012
Thermal infrared radiation	from 30 th March to 1 st April	Coversphere/Atmosphere	Lisi et al., 2010
Thermal infrared radiation	from 30 th to 31 st March	Coversphere/Atmosphere	Genzano et al., 2009
F2-layer critical frequency	16 th March, 5 th April	Ionosphere	Tsolis and Xenos, 2010
Total electron content	2 nd April, 4 th April	Ionosphere	Akhoondzadeh et al., 2010

1010

1011

1012

1013

1014

1015

1016

1017

1018

1019

1020

1021

1022

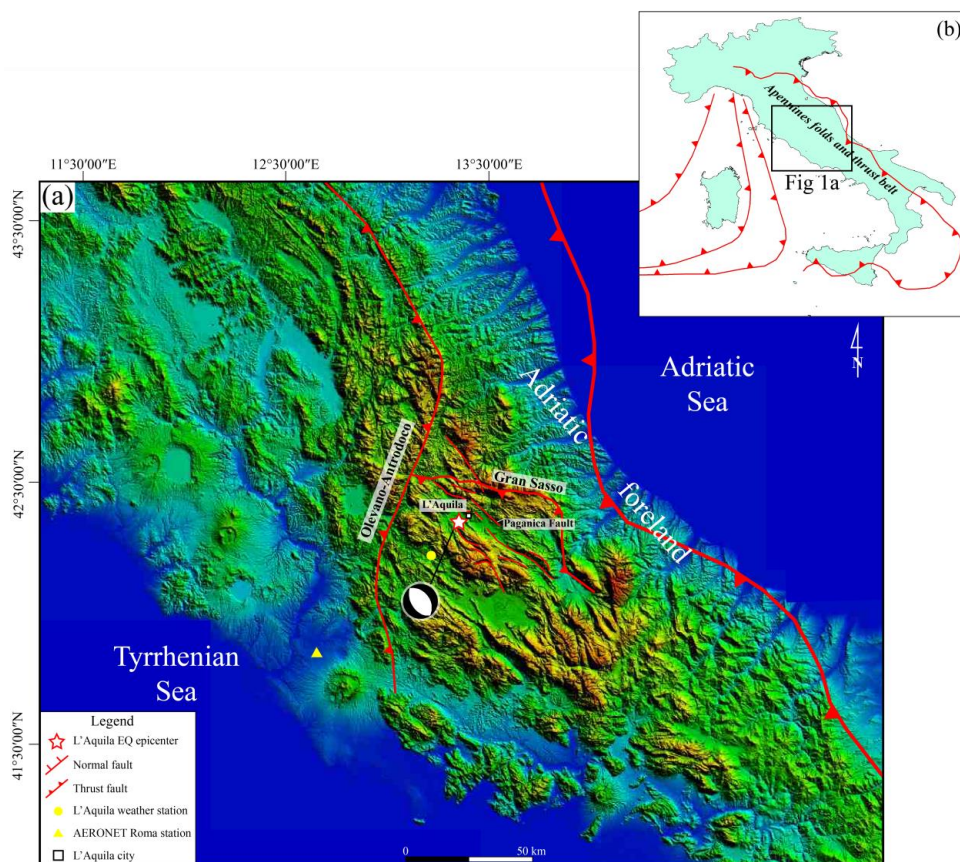
1023



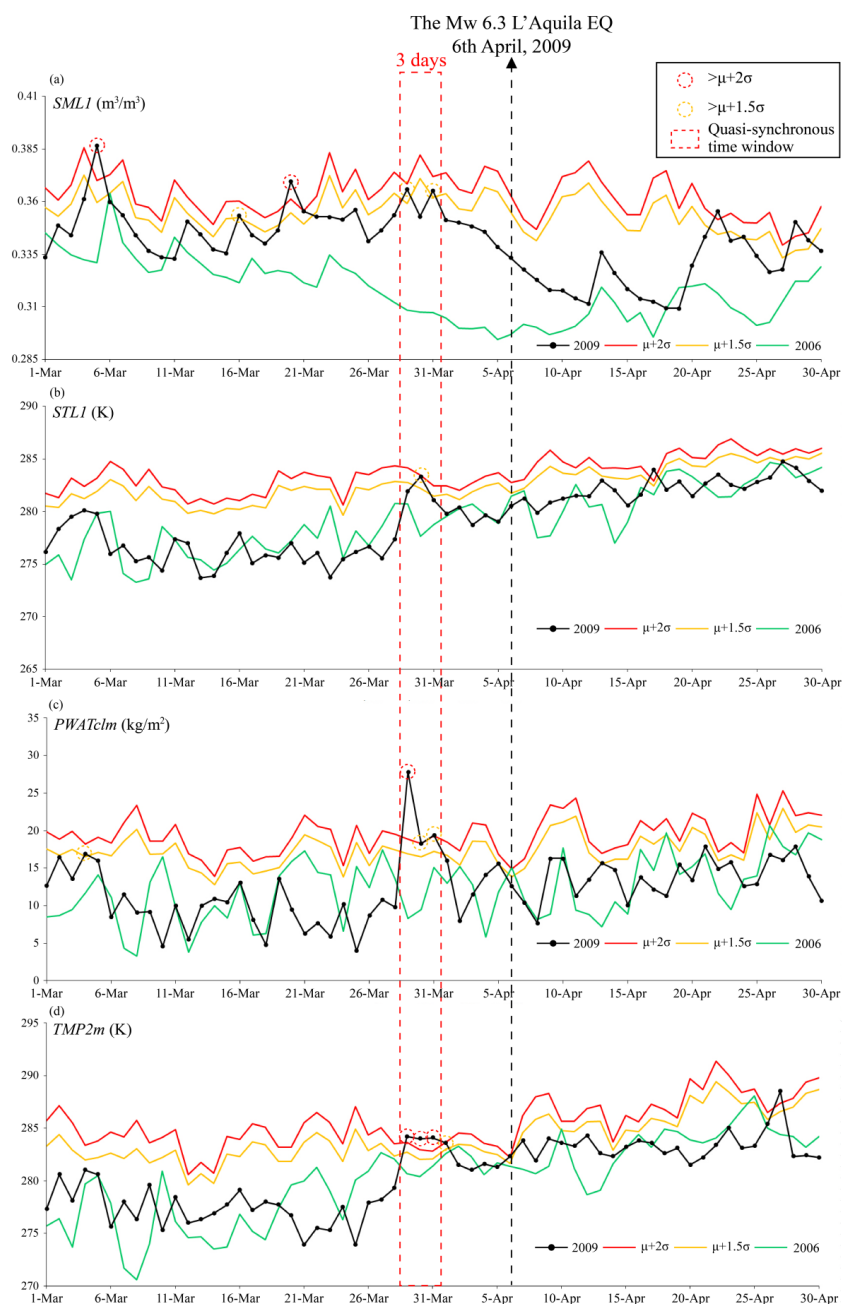
1024 **Table 2** Hydrothermal parameter anomalies from March 29 to April 1, 2009 (quasi-synchronous
 1025 period)

<i>Parameters</i>	<i>Alternative anomaly date</i>	<i>Abnormal deviation</i>		<i>Spatial anomaly</i>
		$> \mu + 1.5\sigma$	$> \mu + 2\sigma$	
SML1 (m ³ /m ³)	March 29	0.007		Strongly concentrated in L'Aquila basin and geo-related to <i>Olevano-AnTRODoco</i> and <i>Gran Sasso</i> thrusts to the north.
	March 31	0.003		Concentrated in L'Aquila basin and geo-related to <i>Olevano-AnTRODoco</i> and <i>Gran Sasso</i> thrusts to the north, but it was smaller and weaker than that on March 29.
STL1 (K)	March 30	1.13		Strongly concentrated on the east of the mainshock with EW trending (crossing the southern part of <i>Olevano-AnTRODoco</i> thrust) and extended to the northwest of the central Italy.
PWATclm (kg/m ²)	March 29		8.97	Strongly covered the entire land and sea of the central and southern Italy and weakly concentrated on the east part of L'Aquila basin (the south of <i>Gran Sasso</i> thrust).
	March 30		0.03	Unapparent
	March 31		0.11	Unapparent
TMP2m (K)	March 29		0.53	Strongly and largely distributed in the northwest of the central Italy (to the west of <i>Olevano-AnTRODoco</i> thrust).
	March 30		1.05	Unapparent
	March 31		1.28	Distributed in the northwest of the central Italy (to the west of <i>Olevano-AnTRODoco</i> thrust), but was smaller and weaker than that on March 29.
	April 1	0.571		Unapparent

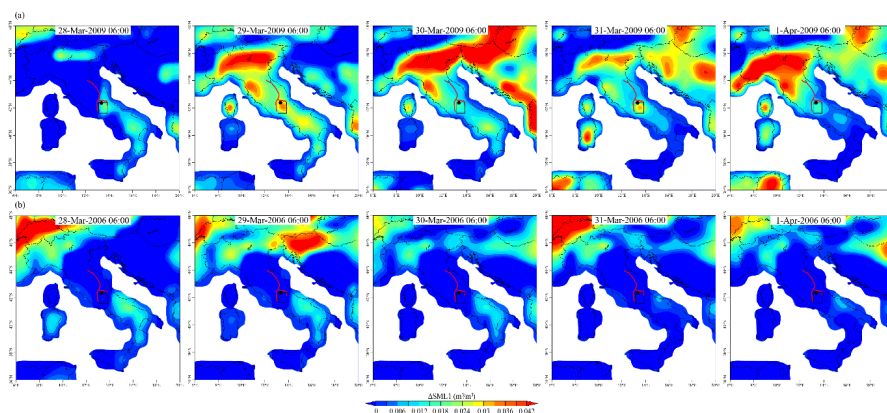
1026



1027
 1028 **Fig. 1** Simplified tectonic and topographic map of central Italy. (a) DEM from the Shuttle Radar
 1029 Topography Mission (SRTM) data showing the epicenter of the 2009 L'Aquila EQ (white star)
 1030 along with its focal mechanism solution (FMS). The FMS was obtained from the US Geological
 1031 Survey's National Earthquake Information Center (Di Luccio et al., 2010; Piroddi et al. 2014). (b)
 1032 The main thrusts in Italy, with the black solid line box showing the geographical location of Fig.
 1033 1a (Benoit et al. 2011).



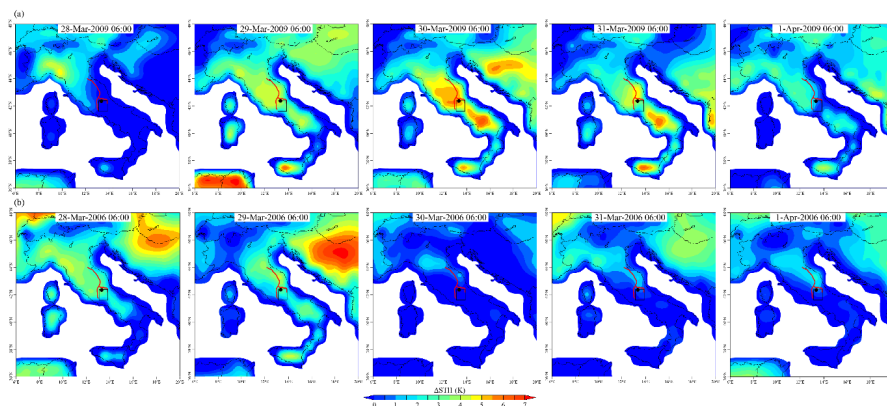
1034
 1035 **Fig 2.1** Time series of four hydrothermal parameters, *SMLI* (a), *STLI* (b), *PWATclm* (c) and
 1036 *TMP2m* (d), on the epicenter pixel from March to April 2009, and its comparison with historical
 1037 data over the same period. The red and orange lines show the value of $(\mu+2\sigma)$ and $(\mu+1.5\sigma)$,
 1038 respectively; the green and black lines show the value in 2006 (as a normal background) and 2009,
 1039 respectively.



1040

1041 **Fig. 2.2** Spatial distributions of $\Delta SML1$ at 06:00 UTC from March 28 to April 1, 2009 (a) and
 1042 2006 (b), respectively. The black spot indicates the epicenter of the main shock, the black
 1043 rectangular box indicates the epicenter pixel, and the red line indicates the related main fault
 1044 system.

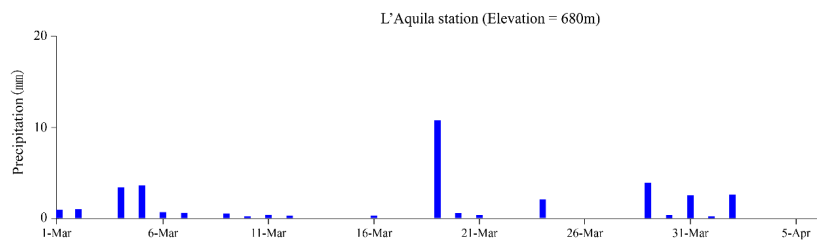
1045



1046

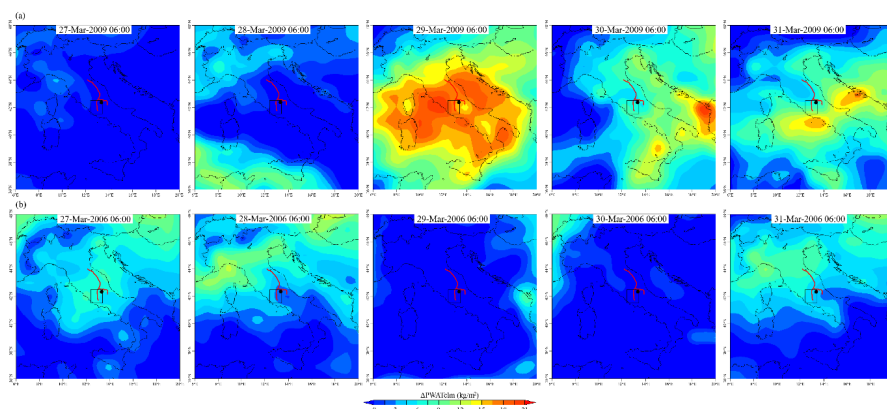
1047 **Fig. 2.3** Spatial distributions of $\Delta STL1$ at 06:00 UTC from March 28 to April 1, 2009 (a) and
 1048 2006 (b), respectively. The black spot indicates the epicenter of the main shock, the black
 1049 rectangular box indicates the epicenter pixel, and the red line indicates the related main fault
 1050 system.

1051



1052

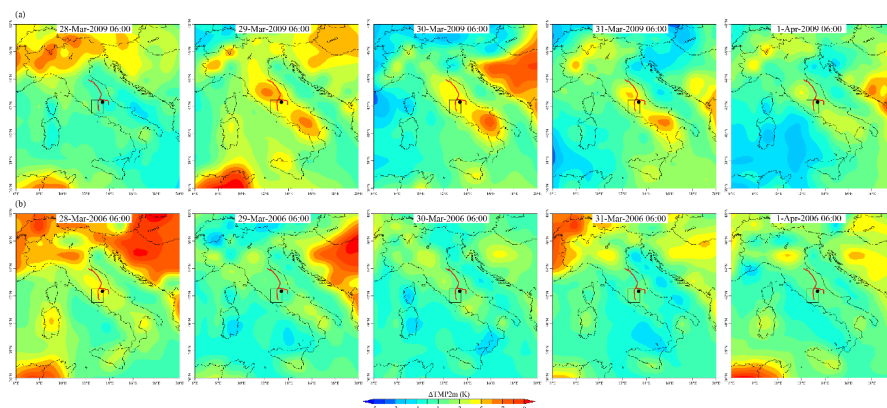
1053 **Fig. 2.4** Daily precipitation at L'Aquila station from March 1 to April 5, 2009.



1054

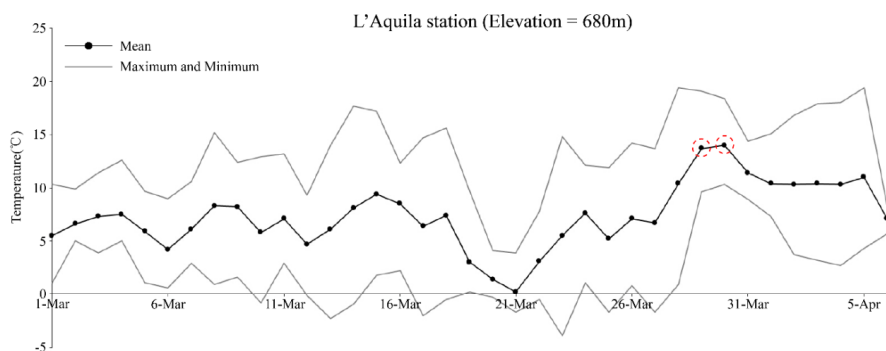
1055 **Fig. 2.5** Spatial distributions of $\Delta PWAT_{elm}$ at 06:00 UTC from March 28 to April 1, 2009 (a) and
1056 2006 (b), respectively. The black spot indicates the epicenter of the main shock, the black
1057 rectangular box indicates the epicenter pixel, and the red line indicates the related main fault
1058 system.

1059



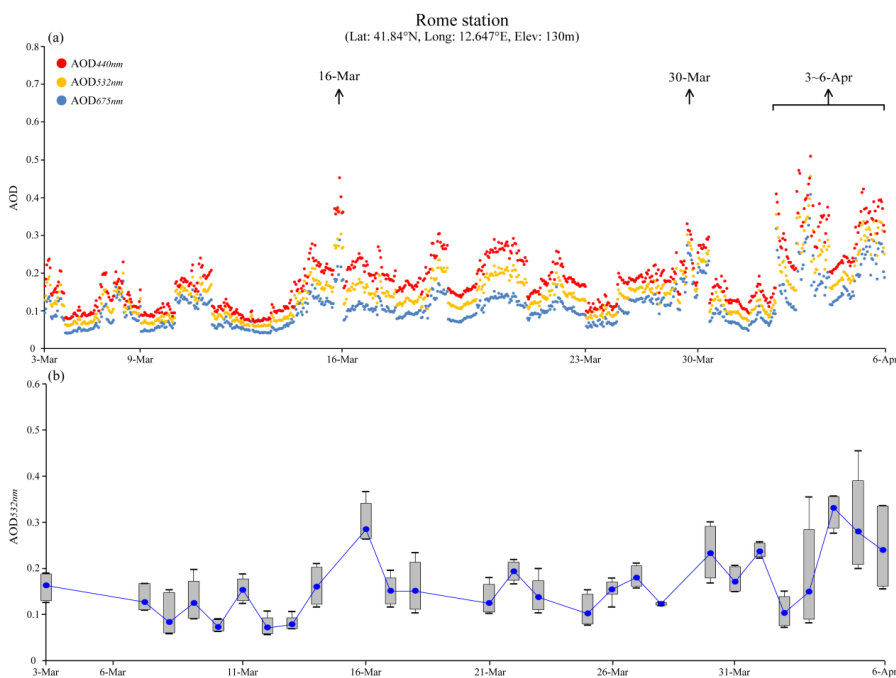
1060

1061 **Fig. 2.6** Spatial distribution of ΔTMP_{2m} at 06:00 UTC from March 28 to April 1, 2009 (a) and
1062 2006 (b), respectively. The black spot indicates the epicenter of the main shock, the black
1063 rectangular box indicates the epicenter pixel, and the red line indicates the related main fault
1064 system.



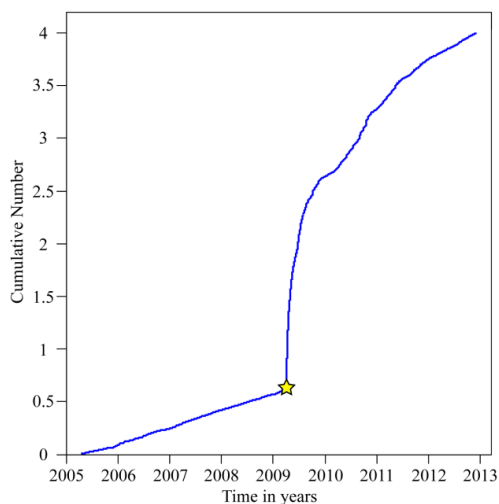
1065
 1066
 1067
 1068

Fig. 2.7 Daily average and maximum and minimum values of air temperature at the L'Aquila station from March 1 to April 5, 2009.

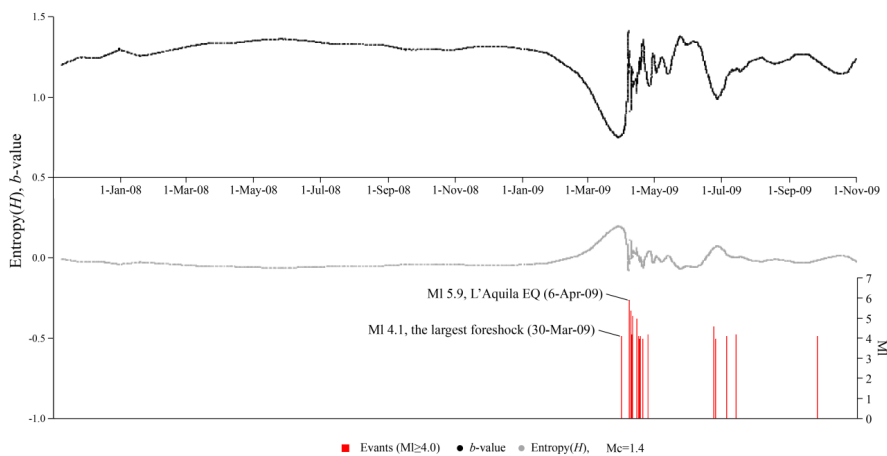


1069
 1070
 1071
 1072
 1073

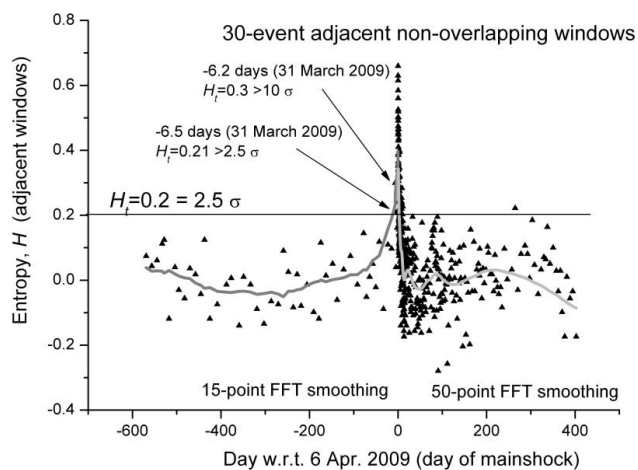
Fig. 2.8 Time series of AOD at the Roma station of AERONET from March 3 to April 6, 2009. (a) AOD at 440, 532, and 675 nm; (b) daily average and maximum and minimum values of AOD_{532nm}, as well as the 5th and 95th percentile box plots.



1074
 1075 **Fig. 3.1** Cumulative number of analyzed catalog as a function of time (the yellow star shows the
 1076 main shock of the 2009 L'Aquila EQ).
 1077

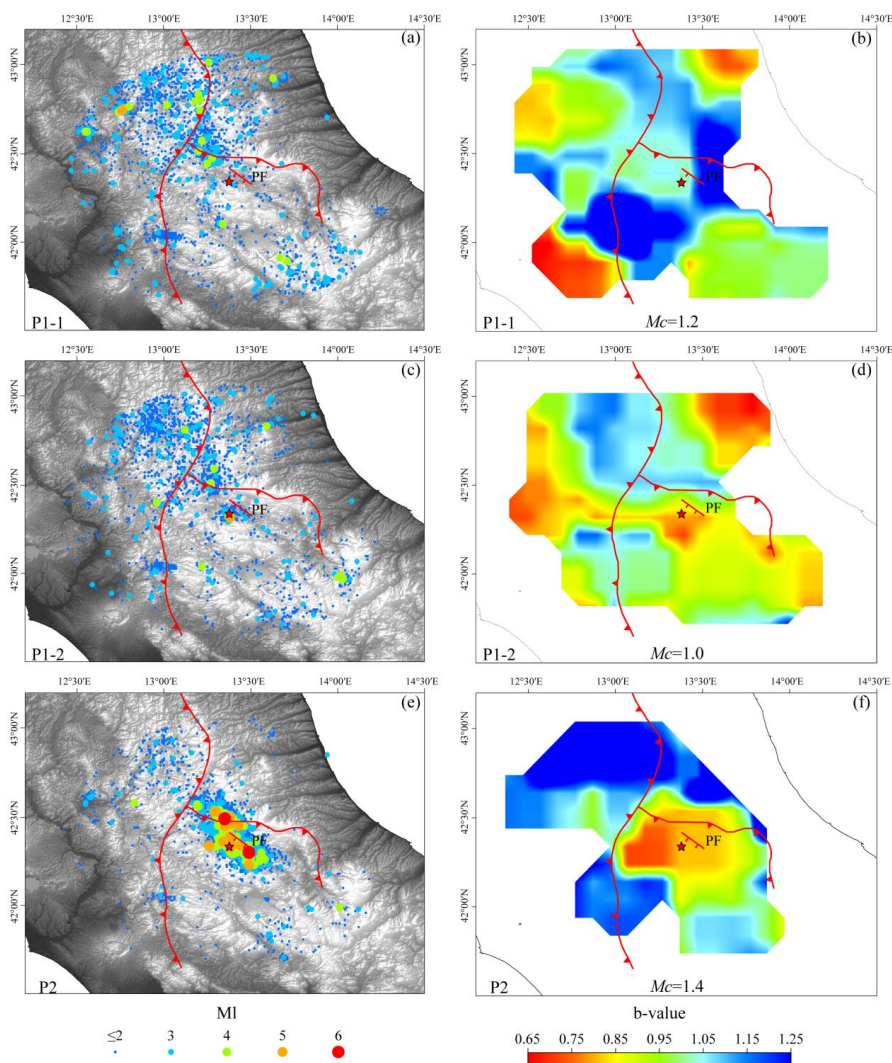


1078
 1079 **Fig. 3.2** Time series of b -value (above plot), Shannon entropy (H ; intermediate plot), and seismic
 1080 events ($M_I \geq 4.0$; bottom plot) during phases P1-2 and P2.
 1081



1082

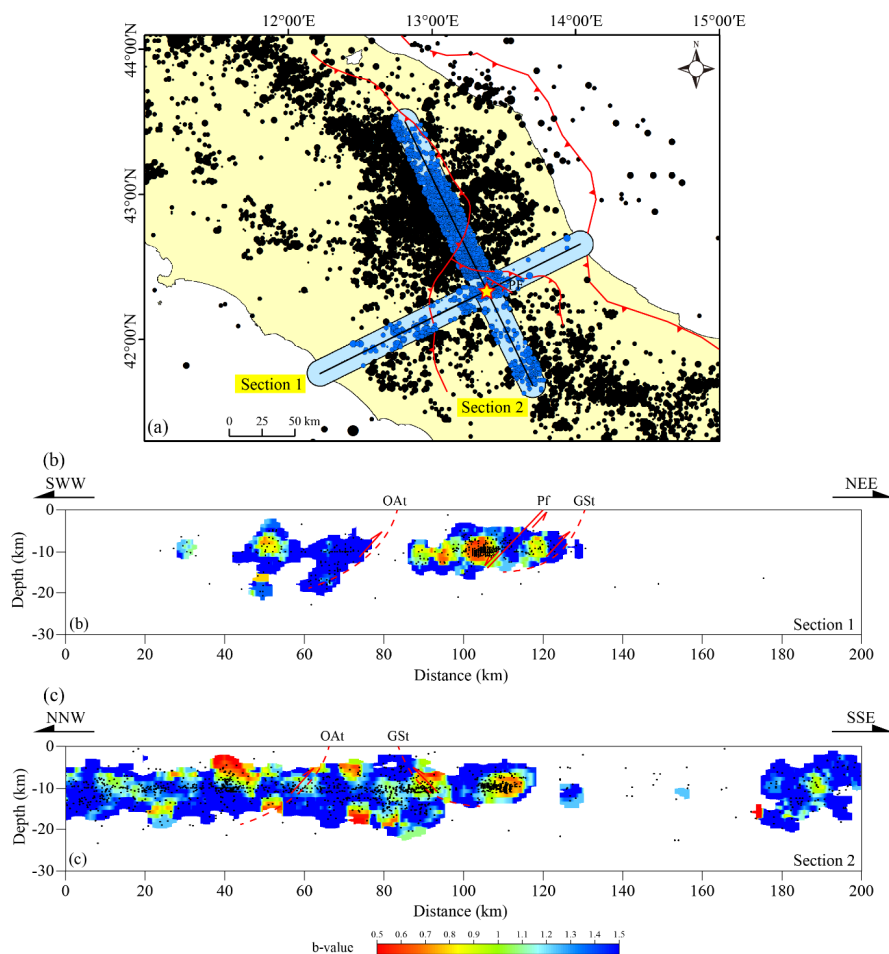
1083 **Fig. 3.3** Shannon entropy for L'Aquila seismic sequence from around 1.5 year before the
1084 mainshock to around 1 year after, calculated for a circular area of 80 km around the mainshock
1085 epicenter. The gray curve defines a reasonable smoothing of the entropy values: 15-point FFT
1086 before the mainshock and 50-point FFT smoothing after the mainshock. Sigma is the standard
1087 deviation estimated over the whole interval.



1088

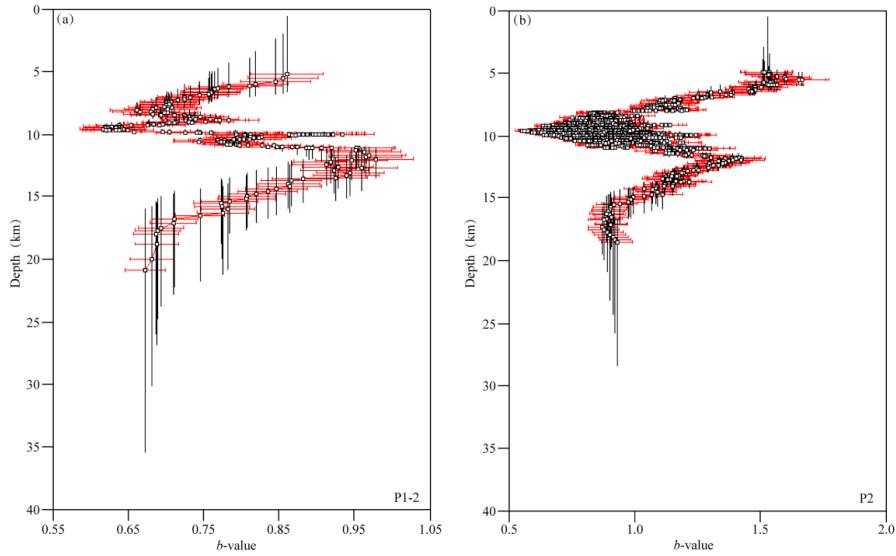
1089 **Fig. 3.4** Spatial distributions of epicenters (a, c, e) and *b*-value (b, d, f) before and after the main
 1090 shock of the L'Aquila EQ at three-staged phases (the red star and the red lines represent the main
 1091 shock and main fault system, respectively).

1092

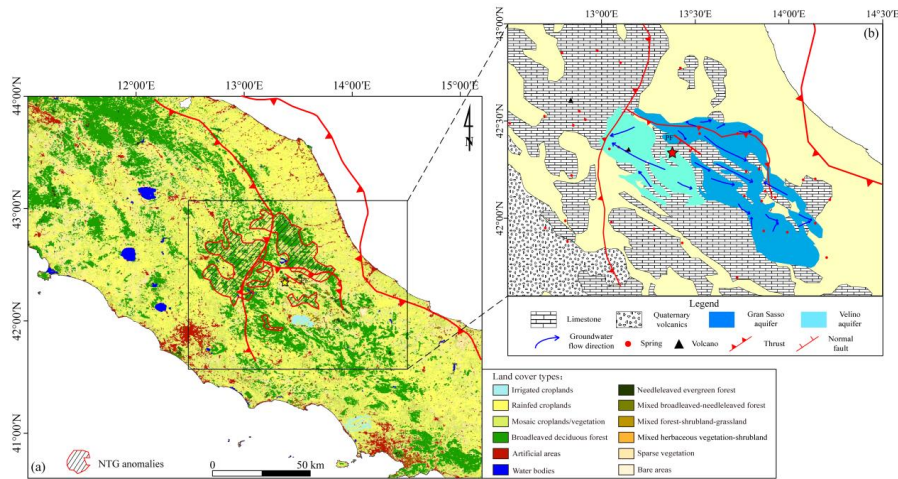


1093

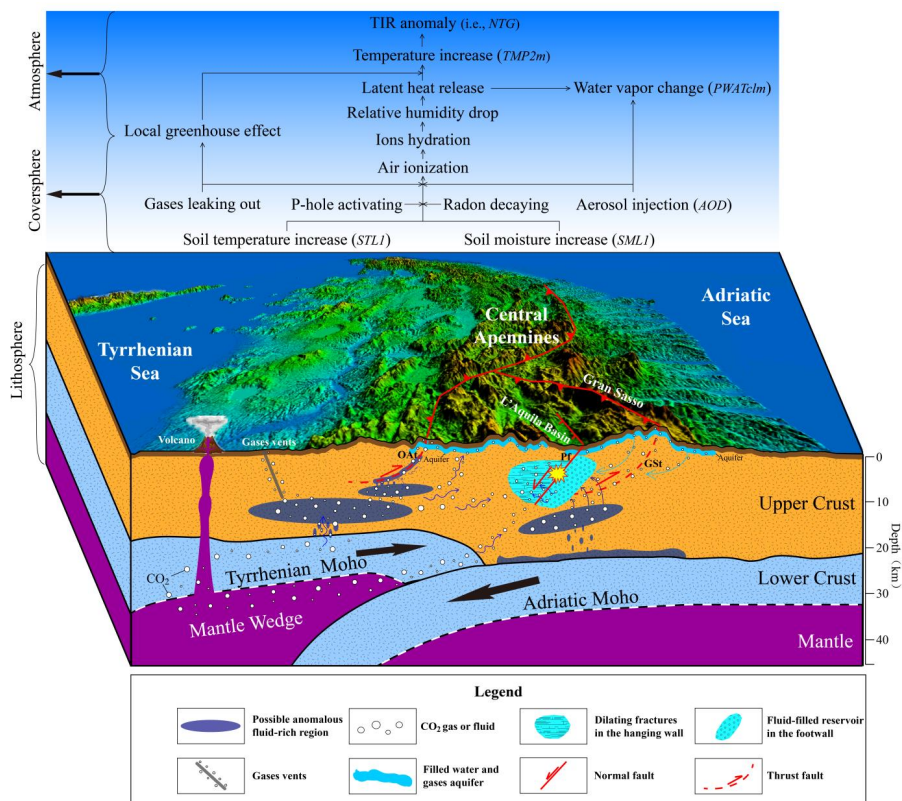
1094 **Fig. 3.5** Spatial distribution of epicenters/hypocenters and b -values from P1-1 to P1-2. (a) The
 1095 outcrops of seismic faults and thrust, as well as all the epicenters of the foreshocks and the main
 1096 shock; (b) b -values along section 1 crossing the main shock epicenter and seismic faults and thrust
 1097 (the black dots represent hypocenters); (c) b -values along section 2 crossing the main shock
 1098 epicenter and seismic faults and thrust (the black dots represent hypocenters). OAt: *Olevano–*
 1099 *Antrodoco* thrust, GSt: *Gran Sasso* thrust, Pf: *Paganica* fault.



1100
 1101 **Fig. 3.6** The relation between the b -values and hypocenter depths in phase P1-2 (a) and phase P2
 1102 (b). The dots indicate the average b -values related to depth, the horizontal bars indicate the
 1103 uncertainty in the b -values, and the vertical bars indicate the depth range of the sampled
 1104 hypocenters.
 1105



1106
 1107 **Fig. 4.1** An integrated representation of the geographical (coversphere) and geological
 1108 (lithosphere) environments associated with the 2009 L'Aquila EQ. (a) Zones of NTG anomalies
 1109 from LST data overlapped by land covers (Piroddi and Ranieri, 2012); (b) the spatial distribution
 1110 of tectonic faults, geological rocks, hydrogeological aquifers, and groundwater flows in the
 1111 epicenter area and its surroundings (Chiodini et al., 2012).



1112

1113 **Fig. 4.2** Mechanism of hydrothermal anomalies and conceptual mode of LCA coupling associated
 1114 with the 2009 Mw 6.3 L'Aquila EQ in Italy (referring to Chiarabba et al., 2010; Chiodini et al.,
 1115 2004; Di Luccio et al., 2010; Lucente et al., 2010; Terakawa et al., 2010). OAt: Olevano–
 1116 Antrodoco thrust, GSt: Gran Sasso thrust, Pf: Paganica fault.